Summer 8-2016

Hybrid Chebyshev Polynomial Scheme for the Numerical Solution of Partial Differential Equations

Balaram Khatri Ghimire
University of Southern Mississippi

HYBRID CHEBYSHEV POLYNOMIAL SCHEME FOR THE NUMERICAL SOLUTION OF PARTIAL DIFFERENTIAL EQUATIONS

by

Balaram Khatri Ghimire

A Dissertation
Submitted to the Graduate School
and the Department of Mathematics
at The University of Southern Mississippi
in Partial Fulfillment of the Requirements
for the Degree of Doctor of Philosophy

Approved:

Dr. Ching-Shyang Chen, Committee Chair
Professor, Mathematics

Dr. Haiyan Tian, Committee Member
Associate Professor, Mathematics

Dr. Huiqing Zhu, Committee Member
Associate Professor, Mathematics

Dr. Zhaoxian Zhou, Committee Member
Associate Professor, School of Computing

Dr. Karen S. Coats
Dean of the Graduate School

August 2016

Published by the Graduate School

ABSTRACT

HYBRID CHEBYSHEV POLYNOMIAL SCHEME FOR THE NUMERICAL SOLUTION OF PARTIAL DIFFERENTIAL EQUATIONS

by Balaram Khatri Ghimire

August 2016

In the numerical solution of partial differential equations (PDEs), it is common to find situations where the best choice is to use more than one method to arrive at an accurate solution. In this dissertation, hybrid Chebyshev polynomial scheme (HCPS) is proposed which is applied in two-step approach and one-step approach. In the two-step approach, first, Chebyshev polynomials are used to approximate a particular solution of a PDE. Chebyshev nodes which are the roots of Chebyshev polynomials are used in the polynomial interpolation due to its spectral convergence. Then, the resulting homogeneous equation is solved by boundary type methods including the method of fundamental solution (MFS) and the equilibrated collocation Trefftz method. However, this scheme can be applied to solve PDEs with constant coefficients only. So, for solving a wide variety of PDEs, one-step hybrid Chebyshev polynomial scheme is proposed. This approach combines two matrix systems of two-step approach into a single matrix system. The solution is approximated by the sum of particular solution and homogeneous solution. The Laplacian or biharmonic operator is kept on the left hand side and all the other terms are moved to the right hand side and treated as the forcing term. Various boundary value problems governed by the Poisson equation in two and three dimensions are considered for the numerical experiments. HCPS is also applied to solve an inhomogeneous Cauchy-Navier equations of elasticity in two dimensions. Numerical results show that HCPS is direct, easy to implement, and highly accurate.

ACKNOWLEDGMENTS

I would like to thank my advisor, Dr. Chen, who has continuously inspired me in the fascinating journey of state-of-the-art meshless methods in scientific computing. Dr. Chen is one of the most influential individuals of my life, whose passion for simple yet very effective ways of finding solutions to problems in scientific computing enabled me to find more optimal paths of solving mathematical problems. Without his continuous support, this work would not have finished in its completness.

I would also like to extend my sincere thanks to Dr. Ding, whose support from the very beginning of the graduate student life always inspired me to go further in this beautiful field of mathematics. I am also deeply grateful to my committee member Dr. Tian for her interest in this work and her input, suggestions and encouragement during the work. I would like to thank from the bottom of my heart to my committee members Drs. Zhu and Zhou for their continuous support and useful feedback in this work. I am very fortunate to have support of my committee members.

I would like to express special thanks to my family members. My parents offered emotional support during this challenging period. My wife, in particular, has been extremely caring and supportive and carried an extra burden in supporting our family so that I could focus on completing this dissertation project. Thanks to my lovely kids Anupa, Ram, and Laxman, I greatly appreciate for your understanding of your papa's academic efforts.

Finally, my thanks goes to all of my friends at USM, my research group members Thir R Dangal, Lei-Hsin Kuo, Daniel Watson, and specially Anup R Lamichhane who were always ready to help me out at any time during the last couple of years.

TABLE OF CONTENTS

LIST OF TABLES

Table

LIST OF ILLUSTRATIONS

Figure

LIST OF ABBREVIATIONS

BEM	-	Boundary Element Method
CFD	-	Computational Fluid Dynamics
CPS	-	Chebyshev Polynomial Scheme
CS-RBF	-	Compactly Supported Radial Basis Function
CTM	-	Collocation Trefftz Method
DEM	-	Discrete Element Method
FDM	-	Finite Difference Method
FEM	-	Finite Element Method
FVM	-	Finite Volume Method
Inv MQ	-	Inverse Multiquadric
LIPS	-	Lagrange Interpolation Polynomial Scheme
LMPS	-	Localized Method of Particular Solutions
MAE	-	Maximum Absolute Error
MFS	-	Method of Fundamental Solutions
MPS	-	Method of Particular Solutions
MQ	-	Multiquadric
PDE	-	Partial Differential Equation
RBF	-	Radial Basis Functions
RMSE	-	Root-Mean-Square Error
SVD	-	Singular Value Decomposition
TM	-	Trefftz Method
TPS	-	Thin-Plate Spline

Chapter 1

INTRODUCTION

1.1 Background

Partial differential equations (PDEs) are mathematical equations used to describe various naturally occurring physical phenomena. More known Examples of the application of PDEs include modeling spring motions and mechanical vibration or describing heat and sound waves, among many. Despite the usefulness of PDEs in solving many real world problems in science and engineering, so called closed-form analytical solutions in most instances are hard to achieve. As a result, numerous numerical approaches to solving PDEs have been proposed over the past centuries. The most well-established methods are finite difference method (FDM) [31, 59], finite volume method (FVM) [38], finite element method (FEM) [60, 61], boundary element method (BEM) and meshless methods [4, 51, 55]. Today FEM has become the most ubiquitous analysis tool in analyzing engineering problems, e.g., solids, fluids, electronics, magnetic or mulitiphysical problems in the fields such as civil engineering, aeronautical engineering, biomechanical engineering, and automotive industries.

Despite the successes, mesh based methods possess some limitations such as mesh generation, slow rate of convergence, spatial dependence, stability, low accuracy, and difficult to implement in complex geometries [4]. In 1990, Edward Kansa developed Kansa method and is considered as the original radial basis function collocation method (RBFCM) [32, 33]. This method is a truly meshless, infinitely differentiable, numerically accurate, stable with high rate of convergence, and spatial independence. Unlike the mesh based methods in which every node has the connectivity to its neighbouring nodes, these points in the meshless methods have no nodal connectivity and hence can handle complex geometries without much difficulty [6]. Many RBFs have been used in the meshless literature, among them thin plate splines, multiquadric (MQ), and Gaussian are the most widely used globally supported RBFs [6, 7, 22, 32, 33]. Polynomials and trigonometric functions have also been used as basis functions [40].

Chebyshev polynomials are a sequence of orthogonal polynomials which can be defined recursively and well documented [3, 54]. In particular, they are widely used in the numerical solution of boundary value problems for partial differential equations with spectral methods

[3, 5, 54]. It is therefore reasonable to approximate a particular solution of a PDE by using Chebyshev polynomials as a basis function on rectangular domains containing the actual domain of the problem. Chebyshev polynomials are used in numerical work because of its property of bounded variation. The local maxima and minima of Chebyshev polynomials on $[-1, 1]$ are exactly equal to 1 and -1 respectively, regardless of the order of polynomials, which makes them valuable for mini-max approximation. Also, orthogonal polynomials can be used to make the polynomial coefficients uncorrelated, to minimize the error, and to minimize the sensitivity of calculations to round off error. The roots of Chebyshev polynomials, also called Gauss-Lobatto nodes, are used in the polynomial interpolation for high order of accuracy [3]. Therefore, many researchers in this filed have used Chebyshev polynomials as a basis function.

Numerical methods have consistently evolved over recent decades and a number of techniques are now available for analyzing physical phenomena. Although some of these methods are generic and can be used in the analysis of different classes of problems, it is impossible to find one specific method that can be considered the best choice for all types of analysis. Thus, it is common to find situations where the best choice is to use more than one method to arrive at an accurate solution and it is necessary to establish efficient strategies for coupling them [50]. Monroe [50] employed one-stage MFS-MPS known as hybrid meshless method to solve various elliptic PDEs and time dependent problems. Nath *et al.* [53] used one-stage MFS-MPS for the steady Navier-Stokes equations in a lid-driven cavity. Devising efficient coupling strategies is, however, not easy and straightforward techniques such as those involving direct coupling between the chosen methods using a single global matrix can lead to ill-conditioning or huge computational cost. One of the common goals of developing meshless methods is to solve a given set of partial differential equations (PDEs) with minimum human and computational costs. Hence, other than the accuracy and efficiency, the simplicity of the developed meshless algorithm is also of great importance. In this dissertation, Chebyshev polynomial is coupled with boundary meshless methods such as the MFS to solve various boundary value problems. The performance of two-step Chebyshev-MFS and Chebyshev-CTM approach, known as two-step hybrid Chebyshev polynomial scheme (HCPS) for solving PDEs with constant coefficients will be studied first. Then, to solve a wide variety of PDEs, the viability of one-step Chebyshev-MFS approach, known as one-step HCPS will be explored in this dissertation.

1.2 Literature Review

Accuracy, efficiency, stability, and simplicity are main considerations for solving partial differential equations. State-of-the-art meshless methods have been proven as effective numerical methods to fulfil these criteria. The meshless methods can be divided into two categories:

- Meshless domain method: In this method, whole computational domain is discretized into randomly distributed points. The Kansa method [32, 33] developed by Edward Kansa, the method of particular solution (MPS) proposed by Chen *et al.* [6, 7] are the well-known domain type meshless methods.

- Meshless boundary method: The nodes are distributed only on the boundary of the computational domain. The MFS [37], the boundary knot method (BKM)[14], and the singular boundary method (SBM) [15] are some of the meshless boundary alone methods. These methods are sometimes called as indirect boundary element methods (BEM) which is a mesh based boundary method [13].

In boundary element methods, the dimension of the problem is reduced by one as only the boundary of the domain of the problem under consideration needs to be discretized. The advantages of these techniques can be fully exploited if the governing differential equation is homogeneous. It is therefore, often desirable to convert an elliptic boundary value problem governed by an inhomogeneous differential equation to one governed by a homogeneous differential equation. This can be achieved using the method of particular solutions (MPS). To describe the MPS, let us consider the following boundary value problem:

$$\mathcal{L}u(x,y) = f(x,y), \ \ (x,y) \in \Omega, \tag{1.1}$$

with Dirichlet boundary condition

$$u(x,y) = g(x,y), \ \ (x,y) \in \partial\Omega, \tag{1.2}$$

and Neumann boundary condition

$$\frac{\partial u(x,y)}{\partial \mathbf{n}} = h(x,y), \ \ (x,y) \in \partial\Omega, \tag{1.3}$$

where $\Omega \subset \mathbb{R}^2$ is a simply connected domain bounded by a simple closed curve $\partial\Omega$, $\mathcal{L}$ is an elliptic differential operator, f, g, and h are given functions, and the function f can be smoothly extended to a rectangular domain containing Ω.

In this dissertation, an approach that combines a particular solution and a boundary method to solve the problem (1.1)-(1.3) is employed. Let $u = u_p + u_h$ be the solution of (1.1)-(1.3) where u_p is the particular solution that satisfies (1.1), but does not necessarily satisfy the boundary conditions (1.2)-(1.3), and its associated homogeneous solution $u_h(x,y)$ satiesfies:

$$\mathcal{L}u_h(x,y) = 0, \ \ (x,y) \in \Omega, \tag{1.4}$$

$$u_h(x,y) = g(x,y) - u_p(x,y), \ \ (x,y) \in \partial\Omega, \tag{1.5}$$

$$\frac{\partial u_h(x,y)}{\partial \mathbf{n}} = h(x,y) - \frac{\partial u_p(x,y)}{\partial \mathbf{n}}, \ \ (x,y) \in \partial\Omega. \tag{1.6}$$

A particular solution satisfies the given differential equation in the infinite domain without necessarily satisfying the given boundary conditions, and hence for a given differential equation it is not unique. In 1967, Fox *et al.* [24] proposed the method of particular solutions for solving the Laplace eigenvalue problem using the combination of Bessel functions and sine functions as basis functions. In the meshless literature, Kansa method [32] is considered as the global RBF collocation method introduced by Edward Kansa in 1990 which suffers from full, dense, and ill-conditioning of matrices. As the earlier version of RBF collocation methods suffer from full, dense, and ill-conditioning of matrices, many RBF collocation methods have been developed to overcome these issues [2, 6, 7, 16]. Researchers in this field developed various localized version of RBF collocation methods and applied extensively to solve large-scale problems that arise in the field of science and engineering. The local Kansa method [39, 65] and the localized method of particular solution [11, 26, 66] are two main categories of the localized RBF collocation methods. These new methods are equally capable to compete with the traditional mesh-based numerical methods such as the FEM and the FDM. Various numerical results and their application in practical problems have proved this fact [53, 66]. While employing method of particular solution, the key issue is to construct the particular solutions $\Phi(r)$ to satisfy the following equation:

$$\mathcal{L}\Phi(r) = \phi(r). \tag{1.7}$$

Typically, there are two approaches to construct the particular solution $\Phi(r)$. One approach is to utilize the RBFs as the basis functions for constructing the particular solution $\Phi(r)$. The other approach is to use the RBFs as the basis functions for approximating $\phi(r)$ and for deriving a particular solution $\Phi(r)$ from (1.7) by reverse differentiation process. Although it is easy to derive a particular solution from the first scheme, it doesn't guarantee the matrix invertibility [19] while the matrix by the second scheme possesses the positive definite property [12]. The Kansa method [32], a popular method in the meshless literature belongs

in the first approach, while the method of particular solution (MPS) proposed by Chen *et al.* [6, 66] belongs in the second approach. In this dissertation, the first approach is employed to obtain a particular solution using Chebyshev polynomials as basis functions.

There exist various approaches using polynomials [10, 11, 17, 28, 34] for the evaluation of approximate particular solutions. Chen *et al.* [11] obtained particular solutions in analytical form for 2D Poisson equation when the source function f is a homogeneous polynomial. Golberg *et al.* [28] implemented the MPS using Chebyshev interpolants for 2D and 3D Helmholtz type equations when the source function is monomial. However, book keeping of the many monomial terms of the approximating polynomial $\hat{f}$ and the particular solutions corresponding to these terms becomes very tedious and inefficient. Chen *et al.* [10] used a finite term geometric series expansion on a differential operator to directly obtain a particular solution corresponding to each Chebyshev polynomials. However, the procedure of the actual implementation is quite cumbersome. As a result, some tedious algebraic operations require symbolic manipulations that impede the computational efficiency. Karageorghis *et al.* [34] derived particular solutions for Poisson and bi-harmonic equations directly using Chebyshev polynomials as basis functions. In [34], they made use of special properties of the second derivatives of Chebyshev polynomials without the need for the expanded form of the polynomials. They need to solve a block matrix system, the dimension of which is big when the degrees of the Chebyshev polynomials used is high. Ding *et al.* [17] proposed a recursive formulation or a matrix free method to derive a particular solution. This method requires the expansion of the approximate source function which is in terms of Chebyshev polynomials. To avoid the expansion of the Chebyshev polynomials, a method is proposed that combines the direct collocation and the reduction of the second order derivative of Chebyshev polynomials. It is easy in coding and implementation and the use of Gauss-Lobatto nodes ensure the spectral convergence for the Chebyshev interpolation. Also, there is no problem of ill-conditioning which occurs when RBF approximations are used.

When a particular solution is found, then the associated homogeneous problem (1.4)-(1.6) is solved by boundary methods including the method of fundamental solution (MFS) and the collocation Trefftz method (CTM). The high accuracy of both the MFS and the Chebyshev polynomial scheme will guarantee the accuracy of the solution of (1.1)-(1.3). The MFS was first proposed in 1964 by Kupradze *et al.* [37] and it has been used for solving various problems. Due to the fact that the MFS requires a fictitious boundary in the solution process, the CTM which is based on T-complete functions [35] and does not require a fictitious boundary for solving the homogeneous problem. However, the resulting linear system will be highly ill-posed by the direct implementation of the CTM and requires

special treatments. Despite of its successes, two-step approach has some limitations such as this can only be used to solve elliptic PDEs with constant coefficients and we must have fundamental solution of the differential operator. Monroe [50] employed one-stage MFS-MPS hybrid method to solve elliptic PDEs with variable coefficients. Due to the use of multiquadric (MQ) and inverse multiquadric (IMQ) RBFs, ill-conditioning of the collocation matrix and choosing suitable shape parameter are some issues still to be addressed. Nath *et al.* [53] successfully employed one-stage MFS-MPS for the steady Navier-Stokes equations in a lid-driven cavity. This opened up the possibility of solving large class of PDEs. In this dissertation, to address the ill-conditioning of the resulting matrices, and uncertainty of choosing suitable shape parameter, hybrid Chebyshev polynomial scheme (HCPS) is proposed. This numerical scheme is applied in two-step approach and one-step approach. This numerical scheme is direct, highly accurate, easy to implement, and opened up the possibility of solving a large class of PDEs in higher dimensions as well. Finally, this dissertation will:

- address the problem of ill-conditioning by implementing Chebyshev polynomials as a basis function.
- explore the two-step hybrid Chebyshev polynomial scheme (HCPS) for the solution of second and fourth order elliptic PDEs with constant coefficients.
- explore the one-step hybrid Chebyshev polynomial scheme (HCPS) for the solution of a wide variety of PDEs in higher dimensions.
- explore the radial basis function collocation method (RBDCM) for solving fourth-order PDEs.

1.3 Synopsis

In this dissertation, a new numerical scheme hybrid Chebyshev polynomial scheme (HCPS) is proposed for solving various types of PDEs which is applied in two approaches, two-step HCPS and one-step HCPS. This numerical scheme is direct, less ill-posed, easy to implement, and highly accurate. Also, this can be easily extended to higher order elliptic PDEs and in higher dimensions as well.

Chapter 2 begins with a review of state-of-the-art meshless methods focusing particularly on the methods and techniques used in this dissertation. The RBF collocation method, known as the Kansa method, is introduced. The method of fundamental solution (MFS) and the collocation Trefftz method (CTM), for solving homogeneous solution, are briefly described.

Leave-one-out cross validation (LOOCV), an algorithm to choose the sub-optimal source location while using the MFS, is then explained in the other section. Following this, method of particular solution (MPS) and both one-stage and two-stage MFS-MPS methods will be discussed briefly.

In Chapter 3, Chebyshev collocation method is presented in detail. Polynomial interpolation is defined followed by interpolation error and Chebyshev polynomial interpolation. In the next portions of Chapter 3, the formulation of two-step and one-step hybrid Chebyshev polynomial scheme (HCPS) is presented in detail. The formulation of Cauchy-Navier equations of elasticity will also be described in this chapter.

Chapter 4 consists of numerical results utilizing two-step hybrid Chebyshev polynomial scheme (HCPS). While utilizing HCPS in two-step approach, we employed approach 1 and approach 2 for the numerical solution of various elliptic PDEs. Both approaches provide highly accurate results. The performance of HCPS using collocation Trefftz method (CTM) is also observed in this chapter. The numerical results for the Franke's benchmark test functions and biharmonic problem are presented in the numerical experiments. The performance of the method of fundamental solution (MFS) over the collocation Trefftz method (CTM) is presented in the last section of this chapter.

Similarly, the numerical results from one-step HCPS are presented in Chapter 5. Various numerical experiments are performed to test the numerical accuracy of the proposed scheme on the problems governed by the Poisson equation and inhomogeneous Cauchy-Navier equations. Additionally, the accuracy and stability of the methods are tested for various types of PDEs with different types of boundary conditions in higher dimensions as well. One-step HCPS is also utilized to solve PDEs with constant coefficients in this chapter. Comparison of Chebyshev collocation method with that of radial basis function collocation methods (RBFCM) such as Kansa method, MPS, and MFS-MPS is also of particular interest to us. Comparison between these two collocation methods (Chebyshev collocation method and RBFCM) has been provided in the next section of the Chapter 5.

Solving fourth-order PDEs is always a challenging task for the researchers in this field. In Chapter 6, the radial basis function collocation method (RBFCM) is used for the numerical solution of fourth-order partial differential equations. Conclusions from the numerical results and possible future works are listed in Chapter 7.

Chapter 2

STATE-OF-THE-ART IN MESHLESS METHOD

2.1 Introduction

The radial basis functions are widely used in application for solving various science and engineering problems including function interpolation and solutions of PDEs. The basic idea of RBF collocation method for interpolation is derived from the piecewise polynomial interpolation using a function of Euclidean distance which is defined as follows [4]:

Definition 2.1.1. Given a set of n distinct data points $x_1, x_2, \ldots, x_n$, and corresponding data values $f_1, \ldots, f_n$, then RBF interpolant is given by

$$u(x) = \sum_{i=1}^{n} \alpha_i \phi(\| x - x_i \|)$$

where ϕ is some radial basis function, $\| \, . \, \|$ represents the Euclidean norm and consequently, coefficients $\{\alpha_i\}_{i=1}^{n}$ are determined by using the interpolation condition $u(x_i) = f_i, \;\; i = 1, 2, \ldots, n$, which leads the following linear system:

$$\mathbf{A}\boldsymbol{\alpha} = \mathbf{f}$$

where the entries of $\mathbf{A}$ are $\alpha_{ij} = \phi(\| x_i - x_j \|)$, $\boldsymbol{\alpha} = [\alpha_1, \alpha_2, \ldots, \alpha_n]^T$ and $\mathbf{f} = [f_1, f_2, \ldots, f_n]^T$.

The following globally supported radial basis functions are widely used in the literature.

Table 2.1: Globally supported RBFs.

Types of basis function	$\phi(r), (r \geq 0)$
Multiquadric (MQ)	$\sqrt{r^2 + c^2}$
Inverse multiquadric (IMQ)	$\frac{1}{\sqrt{r^2 + c^2}}$
Thin plate spline (TPS)	$r^2 \ln(r)$
Gaussian	e^{-cr^2}
Conical	r^{2n-1}

2.2 RBF Collocation Methods

In this section, we will briefly discuss some well-known RBF collocation methods.

2.2.1 The Kansa Method

The Kansa method [32], pioneered by Edward Kansa in 1990, is considered to be the first radial basis function collocation method. This method has been successfully applied to solve linear and nonlinear PDEs in physics, material science, and for many engineering problems. The only geometric property utilized in this method is the distance between points in the computational domain, consequently, extension to higher order dimension do not increase the difficulty of the method [20, 21, 32, 64].

To briefly explain the Kansa Method, we consider the boundary value problem (1.1)-(1.3). The important part of the Kansa method involves approximating the solution u with a linear combination of RBFs, i.e.,

$$\hat{u}(x) = \sum_{j=1}^{N} \alpha_j \phi(\|x - x_j\|), \tag{2.1}$$

where $\{\alpha_j\}_{j=1}^{N}$ are coefficients to be determined. Applying the operators, and utilizing the collocation techniques yield

$$\sum_{j=1}^{N} \alpha_j \mathcal{L}\phi(\|x_k - x_j\|) = f(x_k), \;\; k = 1, 2, \ldots, N_i \tag{2.2}$$

and

$$\sum_{j=1}^{N} \alpha_j \mathcal{B}\phi(\|x_k - x_j\|) = g(x_k), \;\; k = N_i + 1, \ldots, N \tag{2.3}$$

where N_i denotes the number of interior points and the number of boundary nodes is denoted by N_b, i.e., $N = N_i + N_b$. The system (2.2) and (2.3) is a square linear system for which the $\{\alpha_j\}_{j=1}^{N}$ can be obtained using any appropriate linear system solver.

2.2.2 The Method of Particular Solutions (MPS)

Chen *et al.* [6, 7] proposed the method of particular solutions (MPS) by using the particular solution of the chosen RBF with respect to a certain differential operator as the basis function. In the MPS, $\hat{u}(x)$ in (2.1) is replaced by

$$\hat{u}(x) = \sum_{j=1}^{N} \alpha_j \Phi(\|x - x_j\|), \tag{2.4}$$

where

$$\mathcal{L}\Phi(\|x-x_j\|) = \phi(\|x-x_j\|). \tag{2.5}$$

For simple differential operator such as $\mathcal{L} = \Delta$, Φ can be obtained by integrating twice of ϕ with respect to r. For more complicated differential operator, the derivation could be more challenging and we refer readers to Reference [6, 7]. We note that the MPS representation appears similar to the Kansa Method. The main difference between the MPS and the Kansa method is that the MPS uses the corresponding derived particular solution of RBF by reverse differentiation process [6]. Thus, the MPS may have more sound mathematical foundation. Some numerical experiments demonstrate that the MPS outperforms the Kansa method in both stability and accuracy, particularly in the evaluation of partial derivatives [12].

2.2.3 Localized Method of Particular Solutions (LMPS)

Inspired by the idea of compactly supported RBFs (CS-RBFs) and different from the global RBF collocation methods, researchers in this field developed various localized methods to alleviate the ill-conditioning of the resultant matrix, costly dense matrix of the RBF interpolation, and the uncertainty of the selection of the optimal shape parameter [39, 65, 66]. In the localized methods, the resulting matrix would be a sparse matrix which can be solved efficiently.

Let $\{x_i\}_{i=1}^N$ be a set of collocation points in $\Omega \cup \partial\Omega$. For each $x_i \in \Omega$, we choose a nearest neighbor points $\Omega_i = \{x_k^i\}_{k=1}^n$, in which $x_k^i = x_{k(i)}$, denotes the local indexing for each collocation point associated to Ω_i. The construction requires that $\Omega_i \cap \Omega_j \neq \emptyset$ for some $j \neq i$, and $\{x_i\}_{i=1}^N = \cup_i \Omega_i$. We wish to formulate a numerical scheme to approximate $u(x)$ and its derivatives at all the collocation points $\{x_i\}_{i=1}^N$.

Consider the collocation method on the local domain Ω_i, and let $x_i = x_j^i \in \Omega_i$ for some $j \leq n$. Then $u(x_i)$ can be approximated as follows:

$$\hat{u}(x_i) = \sum_{k=1}^{n} \alpha_k^i \Phi(\|x_i - x_k^i\|), \tag{2.6}$$

where n is the number of nearest neighboring points x_k^i surrounding collocation point x_i, including the collocation point itself, α_k^i are coefficients to be determined, $\Phi(x)$ is an RBF.

It is easy to show that Φ is non-singular and the inverse matrix can always be computed given that all the nodal points inside Ω_i are different nodes. The unknown coefficients are written as [66],

$$\alpha^i = \Phi^{-1}\hat{u}^i, \tag{2.7}$$

where

$$\alpha = [\alpha_1, \alpha_2, \ldots, \alpha_n]^T, \;\; \hat{u} = [\hat{u}(x_1^i), \ldots, \hat{u}(x_n^i)]^T$$

Hence $\hat{u}(x_i)$ in terms of $\hat{u}$ is given by,

$$\hat{u}(x_i) = \sum_{k=1}^{n} \alpha_k \Phi(\|x_i - x_k^i\|) = \hat{\Phi}(x_i)\alpha = \hat{\Phi}(x_i)\Phi_n^{-1}\hat{u}_n$$

$$\hat{u}(x_i) = \Psi_n(x_i)\hat{u}, \tag{2.8}$$

where

$$\hat{\Phi}(x_i) = [\Phi(\|x_i - x_1^i, \Phi(\|x_i - x_2^i, \ldots, \Phi(\|x_i - x_n^i], \tag{2.9}$$

and

$$\Psi(x_i) = \hat{\Phi}(x_i)\Phi^{-1} = [\psi_1, \psi 2, \ldots, \psi_n]. \tag{2.10}$$

Let

$$\hat{u}_N = [\hat{u}(x_1), \ldots, \hat{u}(x_N)]^T. \tag{2.11}$$

We reformulate in terms of global $\hat{u}_N$ instead of local $\hat{u}_n$. This can be done by padding the vector $\Psi_n(x)$ with zero entries based on the mapping between $\hat{u}_n$ and $\hat{u}_N$. It follows that

$$\hat{u}(x_i) = \Psi(x_i)\hat{u}, \tag{2.12}$$

where, $\Psi(x_i)$ is an $N \times N$ sparse matrix only having $N \times n$ non zero elements. Substituting above in (2.6) we get a linear sparse system of equations which when solved, we get an approximate solution $\hat{u}$ at all of the collocation points as desired.

2.3 Boundary Collocation Methods

The method of fundamental solution (MFS) is one of the most popular methods in boundary collocation methods which requires fictitious boundary outside the domain to avoid singularities [18]. In this dissertation, we employ the MFS and the collocation Trefftz method (CTM), another boundary type method which does not require fictitious boundary for homogeneous solution. We briefly describe these two boundary methods in the next sections.

2.3.1 Method of Fundamental Solutions

The method of fundamental solutions (MFS) is a popular classical meshless boundary-type method. It is free of mesh and integration, and can be extended to higher dimensions. The MFS was first proposed by Kupradze and Aleksidze [37] for solving certain boundary value problems. The MFS requires only boundary discretization and it shares the same advantages as the BEM over domain discretization methods [18]. The MFS started gaining attention after its numerical implementation was proposed by Mathon and Johnston [47] in

the 1970's. Fairweather *et.al.* [18] applied the MFS for solving various types of boundary value problems (BVPs). However, Golberg and Chen [27] extended the MFS for solving nonhomogeneous problems and time-dependent problems. Gradually the MFS attracted much attention in the science and engineering community. The singularities of the MFS are placed outside the domain. Hence, a fictitious boundary is necessary to show where the singularities are located. In the MFS, the shape and location of the source points are significant to the accuracy of the method. Various efforts have been made for adopting the MFS approach. Different formulations of modified MFS have since been developed so that the fictitious boundary can coincide with the domain boundary. These include regularized meshless method (RMM) in 2005 [68], the modified method of fundamental solutions (MMFS) in 2009 [57], and the boundary distributed source method (BDSM) in 2010 [43]. In these methods, source points can be directly located on the real boundary. However, none of the newer versions of the MFS can be easily implemented like MFS. The MFS is easy to implement and it produces highly accurate results for homogeneous problems.

The implementation of the MFS is direct and easy to understand. The MFS utilizes the fundamental solutions $\phi_F(\mathbf{x})$ which satisfy the governing differential equation of interest (Table 2.2) and we approximate solution $\hat{u}(\mathbf{x})$ which is expressed in terms of boundary points as follows:

$$u(\mathbf{x}) \approx \hat{u}(\mathbf{x}) = \sum_{j=1}^{N} \alpha_j \phi_F \left(\|\mathbf{x} - \mathbf{s}_j\|_2 \right), \qquad \mathbf{x} \in \Omega, \tag{2.13}$$

where $\hat{u}(\mathbf{x})$ is the approximate solution, $\left\{\mathbf{s}_j\right\}_{j=1}^{N}$ are the source points on the fictitious boundary, $\{\alpha_j\}$ are unknown coefficients to be determined. To determine the sub-optimal location of the source points, we use leave-one-out cross validation (LOOCV) method for the MFS [56]. Once the source points have been chosen, the coefficients α_j in (2.13) can be obtained by collocation on the boundary $\partial\Omega$. Some commonly used fundamental solutions of elliptical differential operators in $\mathbb{R}^2$ and $\mathbb{R}^3$ are listed in Table 2.2.

The parameters a_n, and b_n are calculated as follows:

$$\begin{aligned} a_1 &= 1, \qquad a_n = \frac{a_{n-1}}{4(n-1)^2}, \\ b_1 &= 0, \qquad b_n = \frac{1}{4(n-1)^2}\left(\frac{a_{n-1}}{n-1} + b_{n-1}\right), \end{aligned}$$

K_m, $m \in \mathbb{Z}$ denotes the modified Bessel functions of the second kind with order m.
H_0^m, $m \in \mathbb{Z}$ denotes order zero Hankel functions of the m^{th} kind.
J_m, $m \in \mathbb{Z}$ denotes order m Bessel functions of the first kind.
Y_m, $m \in \mathbb{Z}$ denotes order m Bessel functions of the second kind.

Table 2.2: Fundamental Solutions for Various Differential Operators.

$\mathcal{L}$	$G(\rho)$ in $\mathbb{R}^2$	$G(\rho)$ in $\mathbb{R}^3$
Δ	$\ln(\rho)$	$\frac{1}{\rho}$
Δ^2	$\rho^2\ln(\rho)$	ρ
Δ^n	$\rho^{2(n-1)}(a_n\ln(\rho)-b_n)$	$\rho^{(2n-3)}$
$\Delta-\lambda^2$	$K_0(\lambda\rho)$	$\frac{e^{-\lambda\rho}}{\rho}$
$(\Delta-\lambda^2)^2$	$\rho K_1(\lambda\rho)$	$e^{-\lambda\rho}$
$\Delta(\Delta-\lambda^2)$	$K_0(\lambda\rho)+\ln(\rho)$	$\frac{e^{(-\lambda\rho)-1}}{\rho}$
$\Delta^2-\lambda^4$	$-iH_0^{(1)}(\lambda\rho)+\frac{2K_0(\lambda\rho)}{\pi}$	$e^{-\lambda\rho}+e^{(-i\lambda\rho)}$
$(\Delta-\lambda^2)^n$	$\rho^{(n-1)}K_{n-1}(\lambda\rho)$	$\rho^{\frac{n-3}{2}}K_{\frac{n-3}{2}}(\lambda\rho)$
$\Delta+\lambda^2$	$-iH_0^{(2)}(\lambda\rho)$	$\frac{e^{-i\lambda\rho}}{\rho}$
$(\Delta+\lambda)^n$	$\rho^{(n-1)}Y_{n-1}(\lambda\rho)$	$\rho^{\frac{n-3}{2}}J_{\frac{n-3}{2}}(\lambda\rho)$

2.3.2 Collocation Trefftz Method

The Trefftz method [63] was first proposed by E. Trefftz in 1926. It is a boundary-type method. In [35], Kita and Kamiya classified the Trefftz formulation into the indirect and the direct ones. Here, we use the indirect formulation, which is the original one presented by the Trefftz. The solution is approximated by the linear combination of the functions satisfying the governing equation [41]. Those functions are called the T-complete functions. Then, the unknown parameters are determined by the collocation on the boundary. Li *et.al.* named this method as a collocation Trefftz method (CTM) in their book [41]. The algorithm for the CTM requires the explicit form of the T-complete functions. Consider a disk

$$S=\{(r,\theta)|0\le r\le R,\ 0\le\theta\le 2\pi\}.$$

We list below the T-complete functions of a few typical equations in 2D, which are often used in practice [41]. Note that $I_\mu(r)$ and $J_\mu(r)$ are modified Bessel function and Bessel

Table 2.3: List of T-complete function.

PDEs	T-complete function
$\Delta u=0$	$1, r^n e^{in\theta}$
$\Delta u-\lambda^2 u=0$	$I_0(\lambda r), I_n(\lambda r)e^{in\theta}$
$\Delta u+\lambda^2 u=0$	$J_0(\lambda r), J_n(\lambda r)e^{in\theta}$
$\Delta^2 u=0$	$1, r^n e^{in\theta}, r^2, r^{n+2}e^{in\theta}$

function of the first kind respectively, i is the imaginary unit, and r, and θ are the polar co-ordinates.

As an example, let us consider the Laplace boundary value problem,

$$\Delta u(x,y) = 0, \ \ (x,y) \in \Omega, \tag{2.14}$$

$$u(x,y) = g(x,y), \ \ (x,y) \in \partial\Omega^D, \tag{2.15}$$

$$\frac{\partial u(x,y)}{\partial \mathbf{n}} = h(x,y), \ \ (x,y) \in \partial\Omega^N, \tag{2.16}$$

where $\mathbf{n}$ denotes the unit outward normal vector on the boundary and g, and h are given functions.

By the CTM, the solution of the problem (2.14)-(2.16) is

$$u_h \approx \sum_{i=0}^{n} a_i \hat{u}_i,$$

where $\hat{u}_i$ are the T-complete functions given in Table 4.3 satisfying the Laplace equation (2.14). The unknown parameters $\{a_i\}$ are determined by collocation on the boundary. For an interior modified Helmholtz problem, the solution can be expressed as

$$u(r,\theta) = a_0 I_0(\lambda r) + \sum_{i=1}^{m} a_i I_i(\lambda r)\cos(i\theta) + b_i I_i(\lambda r)\sin(i\theta), \tag{2.17}$$

where m is the order of the series solution, and $a_0, a_1, a_2, \ldots, a_m$, $b_1, \ldots, b_m$ are unknown coefficients to be determined. Solving the problem using boundary collocation, we obtain the following linear system of equations:

$$\mathbf{Be} = \mathbf{d} \tag{2.18}$$

where, $\mathbf{B} = \{B_{ij}\}$ is the resulting collocation matrix, $\mathbf{e}$ is the vector of unknown coefficients and $\mathbf{d}$ is the right hand side. The dimension of $\mathbf{B}$ is $M \times (2m+1)$ if the number of boundary points is M.

Here, we would like to emphasize that, the resulting matrix is highly ill-conditioned by the direct implementation of the CTM. Hence, to overcome the ill-posedness of the resulting linear system, Kuo *et. al.* [36] implemented multiple scale Trefftz method and equilibrated matrix concept which is briefly described below.

2.3.3 Multiple Scale CTM and Equilibrated Matrix

To alleviate the ill-conditioning of the linear system (2.18) while implementing the CTM, we incorporate the multiple scale Trefftz method and the equilibrated matrix technique [36]. An equilibrated matrix is a resulting matrix of which all the column norms or row norms are

the same, and under this treatment, the matrix has a significantly reduced condition number. By this method, the series solution (2.17) is replaced with the following form:

$$u(r,\theta) = \widehat{a}_0 \frac{I_0(\lambda r)}{R_0} + \sum_{i=1}^{m} \widehat{a}_i \frac{I_i(\lambda r)}{R_{2i-1}} \cos(i\theta) + \widehat{b}_i \frac{I_i(\lambda r)}{R_{2i}} \sin(i\theta),$$

where

$$\widehat{a}_0 = a_0 R_0, \quad \widehat{a}_i = a_i R_{2i-1}, \quad \widehat{b}_i = b_i R_{2i}, \tag{2.19}$$

and $R_0, R_1, \ldots, R_{2m}$ are the multiple-scale characteristic lengths. The concept of characteristic length was first proposed by Liu [42] to reduce the ill-posedness of the Trefftz method and the MFS for solving Laplace equations. The characteristic lengths are computed by

$$R_{j-1} = \alpha \sqrt{\sum_{i=1}^{M} B_{ij}^2}, \quad j = 1, 2, \ldots, 2m+1.$$

Then, the linear system (2.18) is reduced to the system:

$$\mathbf{Ac} = \mathbf{d}, \tag{2.20}$$

with $\mathbf{A} = \{A_{ij}\}$, and $A_{ij} = B_{ij}/R_{j-1}$. That is, all the column norms of the matrix $\mathbf{A}$ are $1/\alpha$. So, $\mathbf{A}$ is an equilibrated matrix. Since $\mathbf{A}$ is well conditioned, we proceed to compute the linear system (2.20).

2.4 Leave-One-Out Cross Validation

The method of fundamental solution (MFS) is used to solve the homogeneous solution which is highly accurate. The singularities of the MFS are placed outside the domain hence require a fictitious boundary. In the MFS, the shape and location of the source points are significant to the accuracy of the method. While implementing the MFS, source locations can be found in different ways. Chen *et. al.* [9] employed various effective techniques for choosing suitable source locations. Readers can refer to [9] and references cited therein for more detail. In this dissertation, a circle and a same shape boundary is taken as a fictitious boundary. To find the suitable source location of the fictitious boundary, leave-one-out cross validation (LOOCV) is employed.

Rippa [56] used the LOOCV in order to find the sub-optimal source location that provides an accurate approximation while maintaining matrix stability. The algorithm computes the error at a single point then bases the approximation on the remaining data points. The procedure is repeated for each data points. The resulting vector is used to find the sub-optimal source location say r.

First, define $x^{[k]} = [x_1, x_2, \ldots, x_{k-1}, x_{k+1}, \ldots, x_M]^T$, the vector of data points with x_k removed. Then, $\tilde{u}^{[k]}$ is the partial RBF interpolant to u,

$$\tilde{u}(x) = \sum_{j=1}^{M-1} \alpha_j \phi(\|x - x_j^{[k]}\|). \tag{2.21}$$

The approximation of the function at the deleted point is $\tilde{u}^{[k]}(x)$. The error between the approximation and actual function value at x_k is

$$e_k = |u(x_k) - \tilde{u}^{[k]}(x_k)|. \tag{2.22}$$

The accuracy for the entire data set is determined by the norm of the vector of errors $\mathbf{e} = [e_1, e_2, \ldots, e_M]^T$ obtained by removing, in turn, each of the data points and comparing the approximation with the known value at the removed point. The above procedure would be tedious and inefficient. However, Rippa simplified the algorithm and one can calculate the error using the formula,

$$e_k = \frac{\alpha_k}{A_k^{-1}}, \tag{2.23}$$

where α_k is the k^{th} coefficient of $\tilde{u}$ for the entire data set and A_k^{-1} is the k^{th} diagonal element of the inverse of the corresponding interpolation matrix. Once the vector $\mathbf{e}$ is determined by using the formula above, the MATLAB function **fminbnd** can be used to find the relative minimum of the cost function for c. The calling sequence for the cost function is

$$r = fminbnd\{@(c)costeps(c, rbf, DM, rhs), \min c, \max c\},$$

where DM is the distance matrix of the matrix A. $\min c, \max c$ is the interval used to search for the sub-optimal source location r and rhs represents the right-hand side of the equation $Ax = b$.

2.5 The Two-Stage MFS-MPS

To describe the two stage MFS-MPS, we consider the boundary value problem (1.1)-(1.3). In the two-stage MFS-MPS approach, the solution u is split into a particular solution and a homogeneous solution to solve the problem (1.1)-(1.3). Let $u = u_p + u_h$ be the solution of (1.1)-(1.3) where u_p is the particular solution that satisfies (1.1), but does not necessarily satisfy the boundary conditions (1.2)-(1.3), and its associated homogeneous solution $u_h(x, y)$ satisfies (1.4)-(1.6). In this approach, u_p is first approximated by the solutions of (2.5), $\Phi(r)$, as given in Section 2.2.2:

$$\hat{u}_p(x) = \sum_{j=1}^{n_i} \alpha_j \Phi(\|x - x_j\|), \tag{2.24}$$

The unknown coefficients $\{\alpha_j\}_{j=1}^{n_i}$ are determined by solving the following system of linear equations:

$$\sum_{j=1}^{n_i} \alpha_j \mathcal{L}\Phi(\|x_k - x_j\|) = f(x_k),\ k = 1,2,\ldots,n_i. \tag{2.25}$$

Then the homogeneous solution u_h is approximated by fundamental solutions $G(\|x - x_j^s\|),\ j = 1,2,\ldots,n_b$.

$$\hat{u}_h(x) = \sum_{j=1}^{n_b} \beta_j G(\|x - x_j^s\|)), \tag{2.26}$$

where $\{x_j^s\}_{j=1}^{n_b}$ are the source points. The coefficients $\{\beta_j\}_{j=1}^{n_b}$ can be obtained by solving the following system of linear equations:

$$\sum_{j=1}^{n_b} \beta_j \mathcal{B}G(\|x_k - x_j^s\|) = g(x_k) - \hat{u}_p(x_k),\ k = n_i + 1,\ldots,N. \tag{2.27}$$

Therefore, we have a general form of an approximate solutions to (1.1)-(1.3) as follows:

$$\hat{u}(x) = \sum_{j=1}^{n_i} \alpha_j \Phi(\|x - x_j\|) + \sum_{j=1}^{n_b} \beta_j G(\|x - x_j^s\|). \tag{2.28}$$

2.6 The One-Stage MFS-MPS

Monroe [50] recently proposed one-stage MFS-MPS hybrid method for solving large class of PDEs. This method is briefly introduced in this section.

In one-stage MFS-MPS, the solution of a given PDE can be written as the sum of a particular solution and a homogeneous solution. That is, the approximate solution of (1.1)-(1.3) can be written as,

$$\hat{u}(x) = \sum_{j=1}^{n_i} \alpha_j \Phi(\|x - x_j\|) + \sum_{j=1}^{n_b} \beta_j G(\|x - x_j^s\|), \tag{2.29}$$

where $\Phi(\|x - x_j\|),\ j = 1,\ldots,n_i$ is obtained from the solutions of (2.5), and $G(\|x - x_j^s\|),\ j = 1,\ldots,n_b$, is the fundamental solution of the differential operator. Thus, we observe that

$$\mathcal{L}G(\|x - x_j^s\|)) = 0, \quad \forall x \in \hat{\Omega},\ j = 1,\ldots,n_b. \tag{2.30}$$

From (2.29), it follows that

$$\mathcal{L}\hat{u}(x) = \sum_{j=1}^{n_i} \alpha_j \mathcal{L}\Phi(\|x - x_j\|). \tag{2.31}$$

Hence, from (1.1)-(1.3), the coefficients α_j and β_j can be obtained by solving the following linear system of equations:

$$\sum_{j=1}^{n_i} \alpha_j \mathcal{L}\Phi(\|x_k - x_j\|) = f(x_k), \quad k = 1,2,\ldots,n_i, \tag{2.32}$$

$$\sum_{j=1}^{n_i} \alpha_j \mathcal{B}\Phi(\|x - x_j\|) + \sum_{j=1}^{n_b} \beta_j \mathcal{B}\Phi(\|x - x_j^s\|) = g(x_k), \quad k = n_i+1,\ldots,N. \tag{2.33}$$

In one-stage approach, the fundamental solution of differential operator $\mathcal{L}$ and the solution of (2.5) have been used together as a basis function to directly approximate the solution of a partial differential equation. This approach is capable of solving PDEs with variable coefficients and thus, is equally effective as that of Kansa method.

Chapter 3

CHEBYSHEV COLLOCATION METHOD

3.1 Introduction

Chebyshev polynomials are a sequence of orthogonal polynomials which can be defined recursively and well documented [3, 46]. The roots of Chebyshev polynomials, also called Gauss-Lobatto nodes, are used in the polynomial interpolation for high order of accuracy. The resulting polynomial minimizes the problem of Runge's phenomena. It is called minimax polynomial of a function since the polynomial minimizes the maximum error. First five Chebyshev polynomials are shown in Figure 3.1. Chebyshev polynomials of the first kind [46],

$$\begin{aligned} T_0(x) &= 1, \\ T_1(x) &= x, \\ T_2(x) &= 2x^2 - 1, \\ T_3(x) &= 4x^3 - 3x, \\ T_4(x) &= 8x^4 - 8x^2 + 1, \\ T_5(x) &= 16x^5 - 20x^3 + 5x, \\ T_6(x) &= 32x^6 - 48x^4 + 18x^2 - 1, \\ T_{n+1}(x) &= 2xT_n(x) - T_{n-1}(x), \ \ n \in \mathbb{N}. \end{aligned} \tag{3.1}$$

Chebyshev polynomials of the second kind [46],

$$\begin{aligned} U_0(x) &= 1, \\ U_1(x) &= 2x, \\ U_{n+1}(x) &= 2xU_n(x) - U_{n-1}(x), \ \ n \in \mathbb{N}. \end{aligned} \tag{3.2}$$

The explicit formula for Chebyshev polynomials in trigonometric form instead of writing the recursion formula (3.1) is given by the following Lemma:

Lemma 3.1.1. *For $x \in [-1,1]$,*

$$T_n(x) = \cos(n\cos^{-1}x), \quad n \geq 0. \tag{3.3}$$

This Lemma can be proved by using standard trigonometric identities. Readers can refer to [46] and references cited therein for more detail. Thus, the recursive formula for the Chebyshev polynomials of the first kind is given by,

$$\begin{aligned} T_0(x) &= 1, \\ T_1(x) &= x, \\ T_{n+1}(x) &= 2xT_n(x) - T_{n-1}(x), \quad n \geq 1. \end{aligned}$$

The roots of the Chebyshev polynomials, which are also called **Chebyshev nodes** or Gauss-Lobatto nodes are also of particular interest. So, the natural question arises, what are the roots of the Chebyshev polynomial $T_{(n+1)}(x)$? By Lemma (3.1.1),

$$T_{n+1}(x) = \cos((n+1)\cos^{-1}x).$$

The roots of $T_{(n+1)}(x)$, $x_0, \ldots, x_n$, are therefore obtained if

$$(n+1)\cos^{-1}(x_j) = (j+\frac{1}{2})\pi, \quad 0 \leq j \leq n,$$

i.e., the $(n+1)$ roots of $T_{(n+1)}(x)$ are

$$x_j = \cos\left(\frac{2j+1}{2n+2}\pi\right). \tag{3.4}$$

In this numerical scheme, first we approximate the particular solution by a linear combination of the Chebyshev polynomials, then we apply the differential operator and collocate on the Chebyshev nodes. For, it is required to have higher order derivatives of Chebyshev polynomials. The first and second order derivatives of Chebyshev polynomials are expressed in terms of first and second kind of Chebyshev polynomials. The relations between the first kind of Chebyshev polynomials T_n and the second kind of Chebyshev polynomials U_n are as follows:

$$\begin{aligned} T_n(x) &= U_n(x) - xU_{n-1}(x). \\ U_n(x) &= xU_{n-1}(x) + T_n(x). \end{aligned}$$

The first, and second derivatives of the Chebyshev polynomials are given by,

$$\begin{aligned} \frac{dT_n}{dx} &= nU_{n-1}, \\ \frac{d^2T_n}{dx^2} &= \frac{n}{x^2-1}(n+1)(T_n - U_n), \\ \frac{d^2T_n}{dx^2}|_{(x=1)} &= \frac{n^4-n^2}{3}, \\ \frac{d^2T_n}{dx^2}|_{(x=-1)} &= (-1)^n\frac{n^4-n^2}{3}. \end{aligned}$$

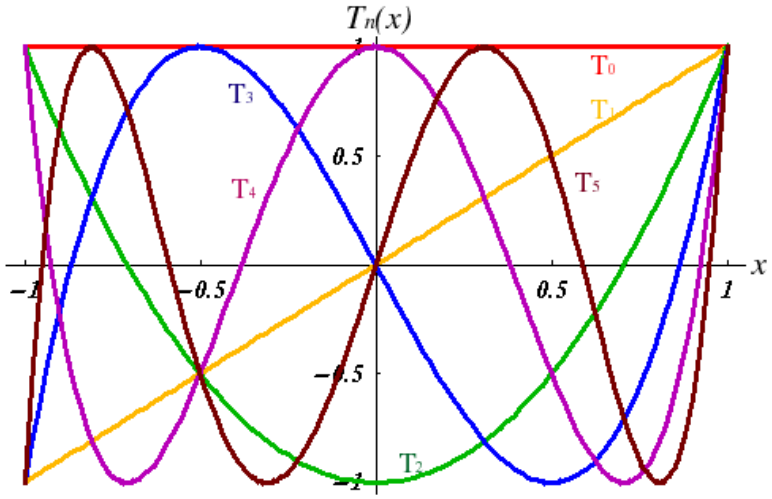

Figure 3.1: Chebyshev polynomial plot.

3.2 The Polynomial Interpolation

Given $n+1$ distinct points $x_0, x_1, \ldots, x_n$, we seek a polynomial $Q_n(x)$ of the lowest degree such that the following interpolation conditions are satisfied [3, 46]:

$$Q_n(x_j) = f(x_j), \quad j = 0, \ldots, n. \tag{3.5}$$

The points $x_0, \ldots, x_n$ are called the **interpolation points**. Here, we are interested in interpolating the data. In other words, given a set of data (measurements and locations at which these measurements were obtained), we want to find a rule (function) which allows us to deduce information about the process we are studying also at locations different from those at which we obtained our measurements [62]. The function that interpolates the data is an **an interpolant** or **an interpolating polynomial**.

3.2.1 The Error in Polynomial Interpolation

In this section, a formula is provided for the error in polynomial interpolation [3, 23, 62]. Since the interpolant and the function agree with each other at the interpolant points, in general, we do not expect them to be close each other elsewhere. So it is required to estimate the difference between them. This difference is referred to as the **interpolation error**. Following theorem estimates the interpolation error. Readers can refer to [62] and references cited therein for the proof of the theorem.

Theorem 3.2.1. *Let $f(x) \in C^{n+1}[a,b]$. Let $Q_n(x) \in \prod_n$ such that it interpolates $f(x)$ at the*

$n+1$ distinct points $x_0, x_1, \ldots, x_n \in [a,b]$. Then $\forall x \in [a,b]$, $\exists \xi_n \in (a,b)$ such that

$$f(x) - Q_n(x) = \frac{1}{(n+1)!} f^{(n+1)}(\xi_n) \prod_{j=0}^{n} (x - x_j). \tag{3.6}$$

3.3 Methodology

In this section, we will first describe two-step hybrid Chebyshev polynomial scheme (HCPS), then one-step HCPS in detail.

3.3.1 Two-Step HCPS formulation

To illustrate the two-step HCPS, we consider the boundary value problem (1.1)-(1.3).

In this approach, the solution u is split into a particular solution and a homogeneous solution to solve the problem (1.1)-(1.3). Let $u = u_p + u_h$ be the solution of (1.1)-(1.3) where u_p is the particular solution that satisfies (1.1), but does not necessarily satisfy the boundary conditions (1.2)-(1.3), and its associated homogeneous solution $u_h(x,y)$ satisfies (1.4)-(1.6). The important part of this method involves the approximation of a particular solution u_p as a linear combination of the Chebyshev polynomials, i.e.,

$$u_p(x,y) \approx \hat{u}_p(x,y) = \sum_{i=0}^{m} \sum_{j=0}^{n} \alpha_{ij} T_i(x) T_j(y), \ (x,y) \in \Omega, \tag{3.7}$$

where $\{\alpha_{ij}\}$ are unknown coefficients to be determined. By collocating on the Gauss-Lobatto nodes $\{x_k, y_k\}_{k=0}^{mn}$, unknown coefficients $\{\alpha_{ij}\}$ can be obtained by solving the following linear system:

$$\sum_{i=0}^{m} \sum_{j=0}^{n} \alpha_{ij} \mathcal{L}\{T_i(x_k) T_j(y_k)\} = f(x_k, y_k). \tag{3.8}$$

Since particular solutions do not necessarily satisfy the boundary conditions, we have the flexibility in extending the domain Ω to a rectangle $[a,b] \times [c,d]$ that contains Ω. Furthermore, we would like to re-scale the domain Ω and the rectangle $[a,b] \times [c,d]$ by the change of variables $\xi = (2x - a - b)/(b-a)$, and $\eta = (2y - c - d)/(d-c)$ so that the new domain $\hat{\Omega}$ is embedded in a square $[-1,1] \times [-1,1]$. The PDE will have to change accordingly in terms of the new variables ξ and η [34].

As an illustration, we consider the following Poisson equation in the (x,y) plane,

$$\Delta u(x,y) = f(x,y), \ (x,y) \in \Omega, \tag{3.9}$$

$$u(x,y) = g(x,y), \ (x,y) \in \partial\Omega. \tag{3.10}$$

By the change of variables,

$$x = \alpha_1 \xi + \beta_1, \;\; y = \alpha_2 \eta + \beta_2,$$
$$\xi = \frac{x-\beta_1}{\alpha_1}, \;\; \eta = \frac{y-\beta_2}{\alpha_2},$$

with

$$\beta_1 = \frac{a+b}{2}, \;\; \beta_2 = \frac{c+d}{2}, \tag{3.11}$$
$$\alpha_1 = \frac{b-a}{2}, \;\; \alpha_2 = \frac{d-c}{2}, \tag{3.12}$$

the problem (3.9)-(3.10) is converted into the following problem in the (ξ, η) plane,

$$\Delta U(\xi, \eta) = F(\xi, \eta), \; (\xi, \eta) \in \hat{\Omega}, \tag{3.13}$$
$$U(\xi, \eta) = G(\xi, \eta), \; (\xi, \eta) \in \partial\hat{\Omega}.$$

We note that $u(x,y) = U(\xi, \eta)$. Hence,

$$\frac{\partial^2 u}{\partial x^2} = \frac{1}{\alpha_1^2} \frac{\partial^2 U}{\partial \xi^2},$$
$$\frac{\partial^2 u}{\partial y^2} = \frac{1}{\alpha_2^2} \frac{\partial^2 U}{\partial \eta^2}.$$

Thus, the original problem (3.9)-(3.10) is transformed into the following problem,

$$\frac{1}{\alpha_1^2} \frac{\partial^2 U}{\partial \xi^2} + \frac{1}{\alpha_2^2} \frac{\partial^2 U}{\partial \eta^2} = f(\alpha_1 \xi + \beta_1, \alpha_2 \xi + \beta_2), \;\; (\xi, \eta) \in \hat{\Omega}, \tag{3.14}$$
$$U(\xi, \eta) = g(\alpha_1 \xi + \beta_1, \alpha_2 \xi + \beta_2), \;\; (\xi, \eta) \in \partial\hat{\Omega}, \tag{3.15}$$

where $\hat{\Omega} \cup \partial\hat{\Omega} = [-1,1] \times [-1,1]$.

For (3.14) to be a Poisson equation, we would like to have $\alpha_1 = \alpha_2$, which is true when $b-a = d-c$ by (3.12). By embedding the original domain $[a,b] \times [c,d]$ into a larger domain $[a_1,b_1] \times [c_1,d_1]$ such that $b_1 - a_1 = d_1 - c_1$, we would be able to achieve this purpose. Consequently, the MFS or the equilibrated CTM are available for the differential operators on the new domain.

The homogeneous solution is approximated by the fundamental solution of the differential operator say $G(\|(x,y;\xi_j,\eta_j)\|)$, where $j = 1, \ldots, N_b$,

$$\hat{u}_h(x) = \sum_{j=1}^{N_b} \beta_j G(\|(x,y;\xi_j,\eta_j)\|), \tag{3.16}$$

where (ξ_j, η_j), $j = 1, \ldots, N_b$ are the source points. The coefficients $\beta_j, j = 1, \ldots, N_b$ can be obtained by solving the following system of linear equations.

$$\sum_{j=1}^{N_b} \beta_j \mathcal{B} G(\|(x_k, y_k; \xi_j, \eta_j)\|) = g(x_k, y_k) - \hat{u}_p(x_k, y_k). \ k = 1, \ldots, N_b. \tag{3.17}$$

Therefore, we have a general form of an approximate solution to (1.1)-(1.3) as follows:

$$\hat{u}(x,y) = \sum_{i=0}^{m} \sum_{j=0}^{n} \alpha_{ij} T_i(x) T_j(y) + \sum_{k=0}^{N_b} \beta_k G(x, y; \xi_k, \eta_k). \tag{3.18}$$

3.3.2 One-Step HCPS Formulation

Let us consider the following elliptic partial differential equation:

$$\mathcal{L}u(x,y) + \alpha(x,y)\frac{\partial u}{\partial x} + \beta(x,y)\frac{\partial u}{\partial y} + \gamma(x,y)u = f(x,y), \ \ (x,y) \in \Omega \tag{3.19}$$

with Dirichlet boundary condition,

$$u(x,y) = g(x,y), \ \ (x,y) \in \partial\Omega_1 \tag{3.20}$$

and Neumann boundary condition,

$$\frac{\partial u(x,y)}{\partial \mathbf{n}} = h(x,y), \ \ (x,y) \in \partial\Omega_2 \tag{3.21}$$

where $\Omega \subset \mathbb{R}^2$ is a simply connected domain bounded by a simple closed curve $\partial\Omega = \partial\Omega_1 \cup \Omega_2$, $\partial\Omega_1 \cap \Omega_2 = \emptyset$. $\mathcal{L}$ is an elliptic differential operator with a known fundamental solution. α, β, γ, f, g, and h are given functions. f is a function that can be smoothly extended to a rectangular domain containing Ω. In this formulation all the terms except the differential operator $\mathcal{L}$ are moved to the right hand side, the resulting equation is

$$\mathcal{L}u(x,y) \ = \ R\left(x, y, u, \frac{\partial u}{\partial x}, \frac{\partial u}{\partial y}\right), \quad (x,y) \in \Omega, \tag{3.22}$$

where

$$R\left(x, y, u, \frac{\partial u}{\partial x}, \frac{\partial u}{\partial y}\right) \ = \ -\alpha(x,y)\frac{\partial u}{\partial x} - \beta(x,y)\frac{\partial u}{\partial y} - \gamma(x,y)u + f(x,y). \tag{3.23}$$

In this one-step method, we assume that the solution can be directly approximated by the sum of the particular solution and homogeneous solution. We approximate the particular solution with a linear combination of the Chebyshev polynomials as follows:

$$u(x,y) \approx \hat{u}(x,y) = \sum_{i=0}^{m}\sum_{j=0}^{n} \alpha_{ij} T_i(x) T_j(y) + \sum_{k=0}^{N_b} \beta_k G(x,y,\xi_k,\eta_k), \tag{3.24}$$

where $\{\alpha_{ij}\}$ and $\{\beta_k\}$ are unknown coefficients to be determined. $\{\xi_j\}_1^{N_b}$ are N_b distinct points on the fictitious boundary $\hat{\Omega}$ of Ω and $G(x,y,\xi_k,\eta_k)$ is the known fundamental solution of the differential operators. Note that due to reformulation of (3.19) into (3.22), we have more than one option for determining the homogeneous solution. Moreover, particular solution is not unique and does not have to satisfy the boundary conditions. So, we can freely embed any irregular domain into a rectangular domain with the change of variables.

In (3.24), two different basis functions were used with two different distance functions to approximate the solution. In this approach, unknown coefficients $\{\alpha_{ij}\}$ and $\{\beta_k\}$ are calculated simultaneously instead of finding them separately as in the two-step approach. To approximate the particular solution, the derivatives of the Chebyshev polynomial is employed for different differential operators.

Using Chebyshev polynomials, the approximation for R is given by,

$$R\left(x,y,u,\frac{\partial u}{\partial x},\frac{\partial u}{\partial y}\right) = \sum_{i=0}^{m}\sum_{j=0}^{n} \alpha_{ij} T_i(x) T_j(y). \tag{3.25}$$

Since $\mathcal{L}G(x,y,\xi_k,\eta_k) = 0$ for $(x,y) \in \Omega$, and by collocation on the Gauss-Lobatto nodes $\{x_k,y_k\}_{k=0}^{mn}$, we have

$$\begin{aligned} \mathcal{L}u \approx \mathcal{L}\hat{u} &= \sum_{i=0}^{m}\sum_{j=0}^{n} \alpha_{ij} \mathcal{L}\{T_i(x_k) T_j(y_k)\} + \sum_{k=0}^{N_b} \beta_k \mathcal{L}G(x,y,\xi_k,\eta_k) \\ &= \sum_{i=0}^{m}\sum_{j=0}^{n} \alpha_{ij} \mathcal{L}\{T_i(x_k) T_j(y_k)\}. \end{aligned} \tag{3.26}$$

Furthermore,

$$\frac{\partial u}{\partial x} \approx \frac{\partial \hat{u}}{\partial x} = \sum_{i=0}^{m}\sum_{j=0}^{n} \alpha_{ij} \frac{\partial}{\partial x}\{T_i(x_k) T_j(y_k)\} + \sum_{k=0}^{N_b} \beta_k \frac{\partial}{\partial x}\{G(x,y,\xi_k,\eta_k)\}. \tag{3.27}$$

$$\frac{\partial u}{\partial y} \approx \frac{\partial \hat{u}}{\partial y} = \sum_{i=0}^{m}\sum_{j=0}^{n} \alpha_{ij} \frac{\partial}{\partial y}\{T_i(x_k) T_j(y_k)\} + \sum_{k=0}^{N_b} \beta_k \frac{\partial}{\partial y}\{G(x,y,\xi_k,\eta_k)\}. \tag{3.28}$$

Using (3.23) and (3.25), the governing equation becomes, for $(x,y) \in \Omega$

$$\sum_{i=0}^{m}\sum_{j=0}^{n} \alpha_{ij} \mathcal{L}\{T_i(x) T_j(y)\} = -\alpha(x,y)\frac{\partial \hat{u}}{\partial x} - \beta(x,y)\frac{\partial \hat{u}}{\partial y} - \gamma(x,y)\hat{u} + f(x,y), \tag{3.29}$$

Now (3.29) can be written as,

$$\sum_{i=0}^{m}\sum_{j=0}^{n}\alpha_{ij}\Psi(x,y)+\sum_{k=0}^{N_b}\beta_k\Theta(\xi_k,\eta_k)=f(x,y), \tag{3.30}$$

where,

$$\begin{aligned}\Psi(x,y) &= \mathcal{L}\{T_i(x)T_j(y)\}+\alpha(x,y)\frac{\partial\{T_i(x)T_j(y)\}}{\partial x} \\ &\quad +\beta(x,y)\frac{\partial\{T_i(x)T_j(y\}}{\partial y}+\gamma(x,y)T_i(x)T_j(y), \end{aligned}\tag{3.31}$$

$$\begin{aligned}\Theta(\xi_k,\eta_k) &= \alpha(x,y)\frac{\partial}{\partial x}\{G(x,y,\xi_k,\eta_k)\}+\beta(x,y)\frac{\partial}{\partial y}\{G(x,y,\xi_k,\eta_k)\} \\ &\quad +\gamma(x,y)G(x,y,\xi_k,\eta_k). \end{aligned}\tag{3.32}$$

The boundary conditions (3.20)-(3.21) become,

$$\sum_{i=0}^{m}\sum_{j=0}^{n}\alpha_{ij}T_i(x)T_j(y)+\sum_{k=0}^{N_b}\beta_kG(x,y,\xi_k,\eta_k) = g(x,y),\ (x,y)\in\Omega_1 \tag{3.33}$$

$$\sum_{i=0}^{m}\sum_{j=0}^{n}\alpha_{ij}\frac{\partial}{\partial\mathbf{n}}\{T_i(x)T_j(y)\}+\sum_{k=0}^{N_b}\beta_k\frac{\partial}{\partial\mathbf{n}}\{G(x,y,\xi_k,\eta_k)\} = h(x,y).\ (x,y)\in\Omega_2 \tag{3.34}$$

Here, Chebyshev polynomials and its successive derivatives evaluated at the Gauss-Lobatto nodes are all known. Hence, an $(mn+N_b)\times(mn+N_b)$ system of equations is formulated as the following system:

$$\begin{bmatrix} A_{11} & A_{12} \\ A_{21} & A_{22} \\ A_{31} & A_{32} \end{bmatrix}\begin{bmatrix} \mathbf{a} \\ \mathbf{b} \end{bmatrix}=\begin{bmatrix} \mathbf{f} \\ \mathbf{g} \\ \mathbf{h} \end{bmatrix}$$

where $A_{11}=\Psi(x,y),\ A_{12}=\Theta(\xi_k,\eta_k),\ A_{21}=\mathbf{T_i}(\mathbf{x})\mathbf{T_j}(\mathbf{y}),\ A_{22}=\mathbf{G},\ A_{31}=\frac{\partial}{\partial\mathbf{n}}\{\mathbf{T_i}(\mathbf{x})\mathbf{T_j}(\mathbf{y})\}$, $A_{32}=\frac{\partial\mathbf{G}}{\partial\mathbf{n}}$. When the coefficients $\{\alpha_{ij}\}$ and $\{\beta_k\}$ are obtained by solving above linear system, then the approximate solution $\hat{u}$ can be determined from (3.24).

3.4 The Cauchy-Navier Equations of Elasticity

We consider the following inhomogeneous Cauchy-Navier equations of elasticity on a unit square.

$$\mu\Delta u_1+\frac{\mu}{1-2\nu}\left(\frac{\partial^2u_1}{\partial x^2}+\frac{\partial^2u_2}{\partial x\partial y}\right)=f_1(x,y),\qquad (x,y)\in\Omega, \tag{3.35}$$

$$\frac{\mu}{1-2\nu}\left(\frac{\partial^2u_1}{\partial x\partial y}+\frac{\partial^2u_2}{\partial y^2}\right)+\mu\Delta u_2=f_2(x,y),\qquad (x,y)\in\Omega, \tag{3.36}$$

subject to the Dirichlet boundary condition:

$$u_1(x,y) = g_1(x,y) \text{ and } u_2(x,y) = g_2(x,y), \quad (x,y) \in \partial\Omega, \tag{3.37}$$

where Ω, and $\partial\Omega$ are domain and its boundary respectively. In the Cauchy-Navier equation, the constant $\nu \in [0,1/2]$ is Poisson's ratio and $\mu > 0$ is the shear modulus.

Now, we briefly describe how we employ one-step HCPS to solve Cauchy-Navier equations of elasticity. Let $\{x_k, y_k\}_{k=1}^{N_b}$ be the source points on the fictitious boundary $\hat{\Omega}$. The approximate solution $(\hat{u}_1, \hat{u}_2)$ of the boundary value problem (3.35)–(3.37) can be approximated by

$$u_1(x,y) \approx \hat{u_1}(x,y) = \sum_{k=1}^{N_b} a_k G(x,y,\xi_k,\eta_k) + \sum_{p=1}^{m}\sum_{q=1}^{n} b_{pq} T_p(x) T_q(y), \tag{3.38}$$

$$u_2(x,y) \approx \hat{u_2}(x,y) = \sum_{k=1}^{N_b} c_k G(x,y,\xi_k,\eta_k) + \sum_{p=1}^{m}\sum_{q=1}^{n} d_{pq} T_p(x) T_q(y), \tag{3.39}$$

where $\{a_k\}, \{b_{pq}\}, \{c_k\}$ and $\{d_{pq}\}$ are unknown coefficients to be determined. $G(x,y,\xi_k,\eta_k)$ is the known fundamental solution of the Laplace operator. Now, applying the fundamental solution of the differential operators and collocating on the known Chebyshev nodes $\{(x_i,y_i)\}_{i=1}^{mn}$, we formulate a system of equations of the order $2(mn+N_b) \times 2(mn+N_b)$. Let $r = \sqrt{(x-x_k)^2 + (y-y_k)^2}$, $1 \le k \le mn$, $(x,y) \in \Omega \cup \partial\Omega$. It follows that

$$\begin{bmatrix} A_{11} & A_{12} & A_{13} & A_{14} \\ A_{21} & A_{22} & A_{23} & A_{24} \\ A_{31} & A_{32} & A_{33} & A_{34} \\ A_{41} & A_{42} & A_{43} & A_{44} \end{bmatrix} \begin{bmatrix} \mathbf{a} \\ \mathbf{b} \\ \mathbf{c} \\ \mathbf{d} \end{bmatrix} = \begin{bmatrix} f_1 \\ f_2 \\ g_1 \\ g_2 \end{bmatrix}$$

where

$$\begin{aligned}
A_{11} &= \frac{\mu}{1-2\nu}\left(\frac{(y-y_k)^2 - (x-x_k)^2}{r^4}\right), \\
A_{12} &= \mu\left(T_p''(x_i)T_q(y_i) + T_p(x_i)T_q''(y_i)\right) + \frac{\mu}{1-2\nu}(T_p''(x_i)T_q(y_i)), \\
A_{13} &= \frac{\mu}{1-2\nu}\left(\frac{-2(x-x_k)(y-y_k)}{r^4}\right), \\
A_{14} &= \frac{\mu}{1-2\nu}\left(T_p'(x_i)T_q'(y_i)\right).
\end{aligned}$$

Also, we have

$$\begin{aligned}
A_{21} &= \frac{\mu}{1-2\nu}\left(\frac{-2(x-x_k)(y-y_k)}{r^4}\right), \\
A_{22} &= \frac{\mu}{1-2\nu}\left(T_p'(x_i)T_q'(y_i)\right), \\
A_{23} &= \frac{\mu}{1-2\nu}\left(\frac{(x-x_k)^2-(y-y_k)^2}{r^4}\right), \\
A_{24} &= \frac{\mu}{1-2\nu}\left(T_p(x_i)T_q''(y_i)\right)+\mu\left(T_p''(x_i)T_q(y_i)+T_p(x_i)T_q''(y_i)\right),
\end{aligned}$$

and

$$A_{31}=A_{43}=\ln(r),\ A_{32}=A_{44}=T_p(x_i)T_q(y_i),\ A_{33}=A_{34}=A_{41}=A_{42}=\mathbf{0}.$$

$$\mathbf{a}=\{a_k\},\ \mathbf{b}=\{b_{pq}\},\ \mathbf{c}=\{c_k\},\text{ and }\ \mathbf{d}=\{d_{pq}\}.$$

Chapter 4

NUMERICAL RESULTS UTILIZING TWO-STEP HCPS

In this section, numerical results obtained from the two-step hybrid Chebyshev polynomial scheme (HCPS) is presented. It is well-known that Chebyshev interpolants provide highly accurate solution subject to the proper node distribution. In this dissertation, Chebyshev polynomial is used as a basis function to approximate the particular solution which is coupled with one of the two well known boundary methods, the method of fundamental solution (MFS) and the collocation Trefftz method (CTM) for solving the elliptic partial differential equations (PDEs). For the MFS, we use the well-known leave-one-out cross validation (LOOCV), a method described in Chapter 2, to determine the sub-optimal source location [56]. We have used several problems with known exact solutions to verify the effectiveness of the proposed method. We carry out the numerical experiments from second to fourth order PDEs. Since the fourth order PDE can be reduced to two second order PDEs, the Chebyshev collocation technique for particular solutions are applicable. While implementing our numerical schemes, it is assumed that the forcing term $f(x,y)$ can be smoothly extended to a rectangular domain which contains the given domain Ω.

Numerical implementation of the hybrid Chebyshev polynomial scheme often yield significantly different results depending on:

- the number of collocation points
- the irregularities of the domains and a number of other possible factors.

In this dissertation, Chebyshev polynomial is used as a basis function which is less ill-posed and free of shape parameter with high rate of convergence. In order to demonstrate the viability of hybrid Chebyshev polynomial scheme in the context of above consideration, some factors must be carefully examined. For example, we have to choose the suitable source location while using the MFS. It is equally important to consider the number of collocating points, i.e. the Chebyshev nodes in this case. When we increase the number of Chebyshev nodes, then the degree of Chebyshev polynomials also increases which might affect the accuracy.

While using the MFS, we let the source points distribute on a circle of radius r. Note that the source radius r is the distance from the geometric center of the domain to anyone of

the source points outside the domain. The source points, $\{(x_s, y_s)\}$, are determined by

$$\begin{aligned} x_s &= a + r * \cos(2\pi i/n_s), \ \ 1 \le i \le n_s \\ y_s &= b + r * \sin(2\pi i/n_s), \ \ 1 \le i \le n_s \end{aligned}$$

where (a,b) is the center of the circle, r is the radius of the circle, and n_s is the number of source points. For the similar placement of fictitious boundary where the source points are located is chosen to have the same shape as that of the boundary. The fictitious boundary (x_s, y_s) are chosen from the physical boundary (x,y) with $(x_s, y_s) = r * (x,y)$ where (x,y) are the boundary points. In the case of three dimensional computational domains, we let the source points distribute on a sphere of radius r in a similar fashion.

To validate the numerical accuracy, we calculate the maximum absolute error (MAE) which is defined as follows:

$$MAE = \max_j \left| (\hat{u}_j - u_j) \right|, \ \ j = 1 \dots q,$$

where q is the number of testing nodes chosen randomly in the domain, $\hat{u}_j$ and u_j denote the approximate solution and the exact solution at the j^{th} node respectively. In the numerical results, N_x and N_y denote Chebyshev nodes in x and y directions respectively.

While implementing hybrid Chebyshev polynomial scheme, it is required to transform the original domain into $[-1,1]^2$, and rescaling of corresponding PDE is necessary so that the MFS and the collocation Trefftz method (CTM) are available for our numerical experiments. This can be accomplished by two different ways which are **Approach 1** and **Approach 2**, say. In both approaches, we first transform the domain into $[-1,1]^2$, and approximate the particular solution using Chebyshev polynomials. After that, in approach 1, we return to our original domain to approximate the homogeneous solution using the MFS and the CTM. However, in approach 2, we work on the transformed domain by rescaling of PDEs and embedding the original domain into a larger rectangular domain so that the MFS and the CTM are available. Both approaches are stable and highly accurate. Numerical experiments applied to different boundary value problems using the MFS and the CTM on various computational domains will be presented in the coming sections. The profile of the original domain and the transformed domain are shown in Figures 4.16, and 4.17 respectively.

4.1 Two-step HCPS

In this section, numerical experiments utilizing two-step hybrid Chebyshev polynomial scheme with Approach 1 and Approach 2 will be given in detail. The computation is carried out on amoeba-shaped, cassini-shaped, peanut-shaped and star-shaped domains.

4.1.1 Poisson Equation, Approach 1

We first consider a Poisson equation with Dirichlet boundary condition:

$$\begin{aligned} \Delta u(x,y) &= f(x,y),\ (x,y) \in \Omega, \\ u(x,y) &= g(x,y),\ (x,y) \in \partial\Omega. \end{aligned} \tag{4.1}$$

The forcing term $f(x,y)$, and the boundary data $g(x,y)$ are generated from the following exact solution:

$$u(x,y) = \cos(3x) - \cos(3y).$$

In Table 4.1, we list the numerical results for this problem with Ω being an amoeba-shaped, cassini-shaped, star-shaped domains. The computational domain Ω as shown in Figure 4.1 is bounded by the curve defined by the following parametric equation:

$$\partial\Omega = \{(x,y) | x = \rho\cos\theta, y = \rho\sin\theta,\ 0 \le \theta \le 2\pi\},$$

where

$$\rho = e^{\sin(\theta)}\sin^2(2\theta) + e^{\cos(\theta)}\cos^2(2\theta).$$

For each domain, 250 uniformly distributed boundary points and 120 randomly selected interior test points are taken for the numerical experiment. We employ the MFS for the evaluation of the homogeneous solution. When using the MFS, we let the source points distribute on a circle of radius r. By LOOCV, the sub-optimal source radii r for the cassini-shaped, amoeba-shaped, peanut-shaped, and star-shaped domains are 1.398, 1.529, 1.985, and 1.493 respectively. Since Chebyshev polynomials provide spectral convergence on the domain $[-1,1]^2$ and the MFS is a highly accurate boundary method, we expect the solution to be highly accurate.

4.1.2 Modified Helmholtz Equation, Approach 1

In this example, modified Helmholtz equation with Dirichlet boundary condition on irregular domains is considered for the numerical accuracy of the proposed scheme employing Approach 1. The governing equation is given by,

$$\begin{aligned} (\Delta - \lambda^2)u(x,y) &= f(x,y),\ \ (x,y) \in \Omega, \\ u(x,y) &= g(x,y),\ \ (x,y) \in \partial\Omega, \end{aligned} \tag{4.2}$$

where $f(x,y)$, and $g(x,y)$ are generated from the following analytical solution:

$$u(x,y) = \cos(3x) - \cos(3y).$$

Table 4.1: Example 1: MAE for Poisson using Approach 1.

Nx=Ny	Amoeba	Peanut	Cassini	Star
10	2.121e-02	2.177e-04	8.658e-04	4.604e-01
12	1.595e-03	7.216e-06	1.612e-05	4.496e-02
14	6.928e-05	1.608e-07	2.862e-07	1.524e-02
16	3.466e-06	4.476e-09	3.055e-09	4.482e-04
18	9.945e-08	4.980e-11	3.574e-11	2.020e-06
20	1.469e-09	1.953e-11	1.979e-13	4.289e-07
22	2.729e-11	4.426e-11	1.951e-13	2.095e-09
24	2.191e-10	6.836e-10	3.570e-13	5.020e-11
26	1.501e-10	1.834e-09	7.918e-13	6.581e-11
28	7.920e-10	3.438e-09	2.633e-12	2.692e-10
30	1.245e-09	2.736e-08	1.485e-11	3.451e-10

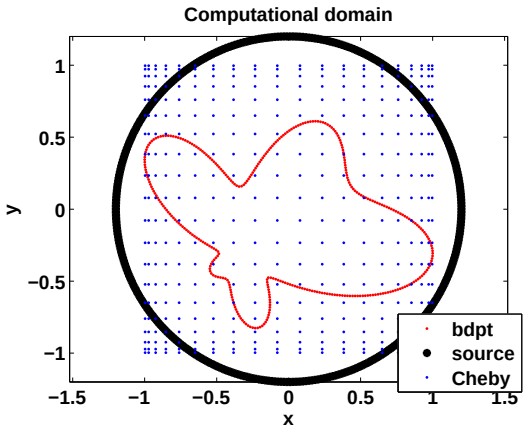

Figure 4.1: The profile of amoeba domain.

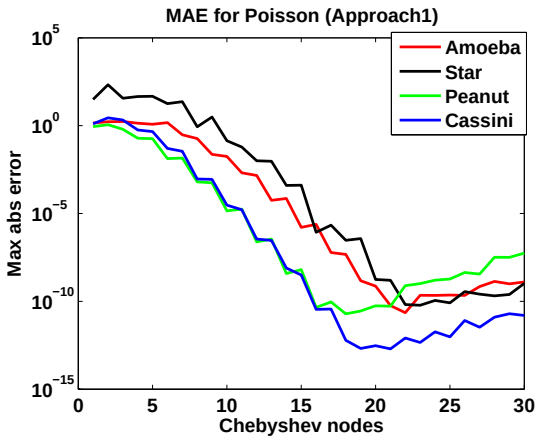

Figure 4.2: The profile of error plot.

The computation domain Ω as shown in Figure 4.3 is bounded by the curve defined by the following parametric equation:

$$\partial\Omega = \{(x,y)|x = \rho\cos\theta, y = \rho\sin\theta,\ 0 \le \theta \le 2\pi\},$$

where

$$\rho = 1 + \cos^2(4\theta).$$

For the MFS, the fictitious boundary where the source points are located is chosen to have the same shape as that of the boundary. The sub-optimal source location in this case is found by using the LOOCV method. The sub-optimal source locations for amoeba-shaped, peanut-shaped, cassini-shaped and star-shaped domains are 1.032, 1.045, 1.022, and 1.056 respectively. For each domain, 250 boundary points and 120 test points are used. The wave number $\lambda = 50$ is used. Table 4.2 shows the numerical result for the two-step hybrid

Chebyshev polynomial scheme. From the numerical results, it can be easily concluded that method is highly accurate and performs better than Poisson equation.

Table 4.2: Example 2: MAE for Helmholtz with approach 1.

Nx=Ny	Amoeba	Peanut	Cassini	Star
10	1.321e-02	7.937e-04	1.987e-04	3.159e-02
12	9.595e-04	2.879e-05	5.206e-06	2.363e-03
14	5.168e-05	7.484e-07	9.868e-08	1.245e-04
16	1.876e-06	1.476e-08	1.285e-09	4.895e-06
18	6.645e-08	2.226e-10	1.374e-11	1.492e-07
20	1.769e-09	2.714e-12	1.158e-13	3.632e-09
22	3.729e-11	2.004e-13	5.440e-15	7.221e-11
24	9.233e-13	9.707e-14	7.772e-15	1.197e-12
26	2.501e-14	1.407e-12	5.690e-15	2.486e-14
28	8.104e-15	7.958e-12	5.718e-15	1.663e-14
30	3.345e-14	4.028e-11	6.726e-15	2.051e-14

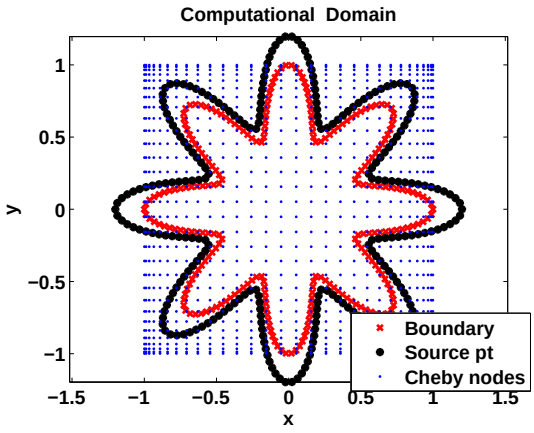

Figure 4.3: The profile of Star shape.

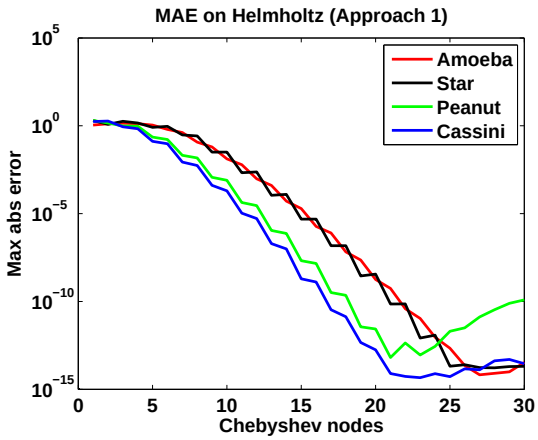

Figure 4.4: The profile of error plot.

4.1.3 Poisson Equation, Approach 2

The governing equation is given by (4.1). We use the MFS for the homogeneous solution. We let the source points distribute on a circle of radius r outside the domain. The well-known LOOCV method is used to find the sub-optimal source radius r. The source radii for amoeba-shaped, cassini-shaped, peanut-shaped, and star-shaped domains are $1.529, 1.398, 2.105$, and 1.510 respectively. Table 4.3 shows the numerical result for the Poisson equation with the second approach. The proposed method is highly accurate and stable. It is noted that as the number of Chebyshev nodes increases, the degree of the Chebyshev polynomials also

increases simultaneously. The highest accuracy is achieved at different Chebyshev nodes for the different domains.

Table 4.3: Example 3: MAE for Poisson with approach 2.

Nx=Ny	Cassini	Peanut	Amoeba	Star
10	1.640e-03	3.807e-03	4.163e-02	1.487e-02
12	4.034e-05	1.982e-04	2.832e-03	1.948e-03
14	9.067e-07	5.417e-06	1.396e-04	5.825e-05
16	1.199e-08	1.149e-07	6.705e-06	8.059e-07
18	1.601e-10	1.991e-09	2.369e-07	8.566e-08
20	1.210e-12	2.053e-11	3.761e-09	3.997e-10
22	8.099e-14	2.605e-13	7.876e-11	1.778e-11
24	1.922e-13	5.467e-14	1.213e-12	3.102e-10
26	1.842e-13	7.965e-14	4.833e-13	9.897e-10
28	6.796e-13	1.446e-13	9.527e-13	1.509e-09
30	1.524e-13	1.469e-13	1.169e-12	9.734e-09

4.1.4 Modified Helmholtz Equation, Approach 2

The governing equation is given by (4.2). We use the MFS for the evaluation of the homogeneous solution. The source points are chosen to have the same shape as that of the physical boundary, and the LOOCV is used to find the sub-optimal source location. Using the LOOCV, the sub-optimal source location for cassini-shaped, peanut-shaped, amoeba-shaped, and star-shaped domains are 1.010, 1.034, 1.043, and 1.051 respectively. For each domain, 250 boundary points and 120 test points are used. The wave number $\lambda = 50$ is used. Table 4.4 shows the numerical result for the two-step HCPS with the second approach.

Table 4.4: Example 4: MAE for Helmholtz with approach 2.

Nx=Ny	Cassini	Peanut	Amoeba	Star
10	4.809e-04	1.586e-03	1.806e-02	3.199e-02
12	1.328e-05	5.757e-05	1.396e-03	2.401e-03
14	2.689e-07	1.496e-06	8.737e-05	1.269e-04
16	4.256e-09	2.924e-08	3.464e-06	5.005e-06
18	4.819e-11	4.452e-10	1.148e-07	1.530e-07
20	4.028e-13	5.431e-12	3.741e-09	3.736e-09
22	1.346e-14	9.064e-14	1.129e-10	7.452e-11
24	8.937e-15	5.104e-14	3.365e-12	1.238e-12
26	7.799e-14	4.873e-14	9.525e-14	1.820e-14
28	7.494e-15	1.887e-14	1.050e-13	2.231e-14
30	1.527e-14	7.904e-14	9.564e-14	2.907e-14

Comparison of the numerical accuracy (error plot) of the second approach applied to Poisson and Helmholtz equation is shown on the Figures 4.5 and 4.6.

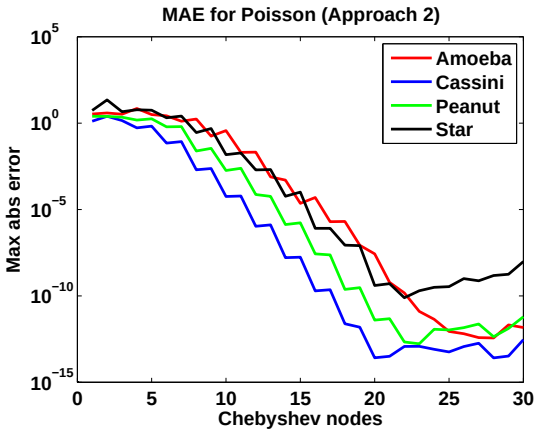

Figure 4.5: The profile of error plot for Poisson equation.

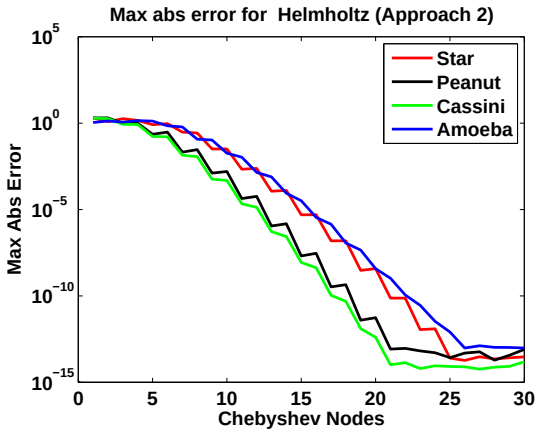

Figure 4.6: The profile of error plot for modified Hemholtz equation.

From the numerical results obtained from the Poisson and the modified Helmholtz equations, it can be easily observed that second approach performs slightly better than the first approach. So, it can be inferred that these two approaches are, in fact, equivalent. Keeping this in mind, in this dissertation, we have employed second approach for the further verification of the proposed hybrid Chebyshev polynomial scheme to solve various elliptic PDEs in 2D and 3D. It is noted that similar accuracy will be achieved by the use of first approach too.

4.1.5 HCPS on Circle

While implementing our numerical scheme, we used different irregular computational domains for the numerical experiments such as amoeba-shaped, cassini-shaped, star-shaped domains and unit square. We also employed our scheme on the circle. Circle is considered as a regular and smooth boundary domain. Table 4.5 is the numerical result for the different Chebyshev nodes on the circle of radius 1 as a physical domain Ω and a circle of radius 1.2 as a fictitious boundary. As in the previous examples, the MFS is employed for the homogeneous solution. 250 uniformly distributed boundary points and 120 randomly distributed test points are taken for the numerical experiment. Due to smooth and regular boundary, we observe highly accurate and stable solutions on the Poisson and modified Helmholtz equations.

Table 4.5: Example 5: MAE for Poisson and Helmholtz on Circle.

Cheby Nodes	Poisson	Helmholtz
Nx=Ny	Maximum Abs Error	Maximum Abs Error
10	2.711e-06	8.343e-07
12	5.458e-08	1.057e-08
14	2.643e-10	1.008e-10
16	3.836e-12	6.042e-13
18	9.325e-15	5.551e-15
20	2.164e-15	6.217e-15
22	1.942e-15	6.217e-15
24	2.665e-15	7.271e-15
26	1.776e-15	4.329e-15
28	1.776e-15	6.911e-15
30	1.487e-12	8.319e-15

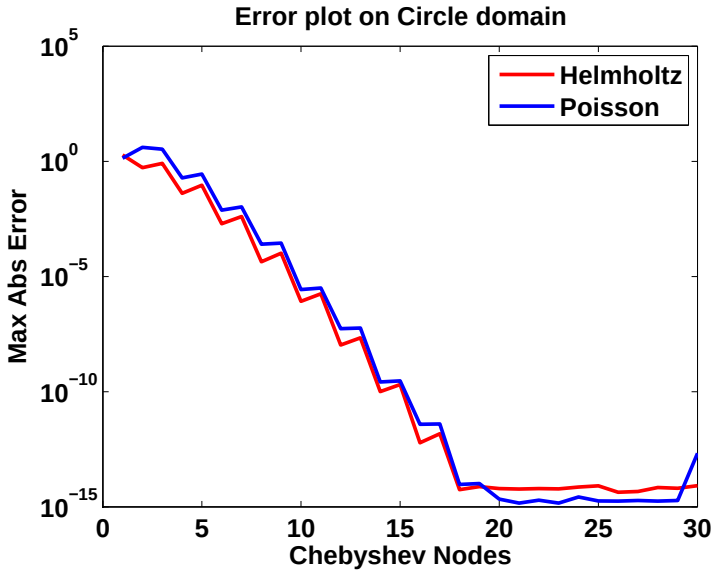

Figure 4.7: MAE for Poisson and Helmholtz on circle.

4.1.6 HCPS Using Mixed Boundary Conditions

To verify the accuracy of numerical methods, we use Neumann boundary condition along with the Dirichlet boundary condition, which is called mixed boundary conditions. In this section, Poisson equation with mixed boundary conditions is presented to verify the numerical accuracy of our proposed method. The computational domains are amoeba-shaped, cassini-shaped and unit square.

$$\begin{aligned} \Delta u(x,y) &= f(x,y), \ (x,y) \in \Omega, \\ u(x,y) &= g_1(x,y), \ (x,y) \in \partial\Omega_1, \\ \frac{\partial u(x,y)}{\partial \mathbf{n}} &= g_2(x,y), \ (x,y) \in \partial\Omega_2, \end{aligned} \tag{4.3}$$

where $\partial\Omega_1$ and $\partial\Omega_2$ are part of the boundary $\partial\Omega$ with $\partial\Omega_1 \cup \partial\Omega_2 = \partial\Omega$ and $\partial\Omega_1 \cap \partial\Omega_2 = \emptyset$, the forcing term and boundary data are obtained from the following analytical solution:

$$u(x,y) = \sin(\pi x)\cos\left(\frac{\pi y}{2}\right).$$

The computational domain is bounded by the cassini curve as shown in Figure 4.8, which is defined by the following parametric equation:

$$\partial\Omega = \{(x,y) | x = \rho\cos\theta, y = \rho\sin\theta, \ 0 \le \theta \le 2\pi\},$$

where

$$\rho = \left(\cos(3\theta) + \sqrt{2 - \sin^2(3\theta)}\right)^{\frac{1}{3}}.$$

In this example, $\partial\Omega_1$ and $\partial\Omega_2$ are the upper and lower half of the boundary $\partial\Omega$ respectively. For the MFS, we use a circle as a fictitious boundary and the well-known LOOCV method is used to find out the sub-optimal source location r. The sub-optimal source location for the amoeba, cassini and unit square are 1.48, 1.96, and 1.87 respectively. The number of boundary and test points are 250 and 120 respectively for amoeba and cassini whereas 276 and 64 for unit square. The profile of error is shown in Figure 4.9. The numerical results shown in Table 4.6 clearly indicate the high accuracy of the proposed method.

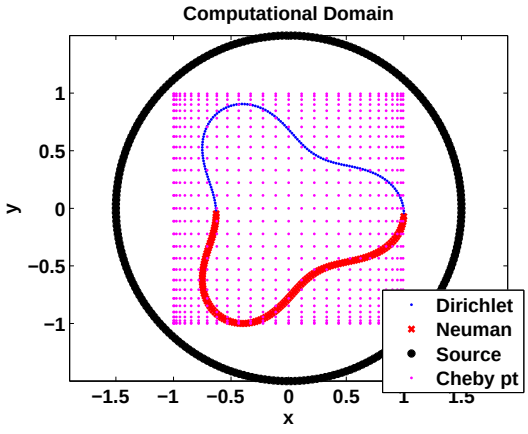

Figure 4.8: The profile of cassini domain

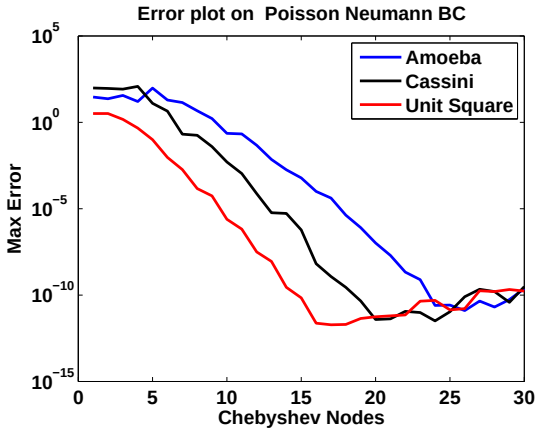

Figure 4.9: Error Plot on mixed BCs.

Table 4.6: Example 6: MAE for Poisson with Mixed BCs.

Nx=Ny	Cassini	Unit Square	Amoeba
10	1.266e-02	7.975e-05	5.430e-01
12	1.958e-04	1.920e-06	7.188e-02
14	3.565e-06	1.946e-08	2.700e-03
16	9.362e-08	2.457e-10	2.683e-04
18	1.832e-10	3.198e-12	1.375e-05
20	3.204e-12	4.559e-12	8.764e-07
22	6.902e-12	6.130e-12	9.825e-09
24	9.390e-12	1.154e-11	2.340e-11
26	2.390e-11	5.784e-11	6.443e-12
28	3.613e-11	1.606e-10	2.490e-13
30	8.021e-10	1.922e-10	1.469e-13

4.1.7 Franke's Benchmark Test Functions

In this example, we consider the cases when three Franke's benchmark test functions [25] are the exact solutions for the Poisson equation and modified Helmholtz equation on the unit square. The three Franke's test functions are given below:
1. F1:

$$\begin{aligned} F1(x,y) &= \frac{3}{4}e^{-\frac{1}{4}[(9x-2)^2+(9y-2)^2]} + \frac{3}{4}e^{-\frac{1}{49}[(9x+1)^2-\frac{1}{10}(9y+1)^2]} \\ &\quad + \frac{1}{2}e^{-\frac{1}{4}[(9x-7)^2-\frac{1}{4}(9y-3)^2]} - \frac{1}{5}e^{-[(9x-4)^2-(9y-7)^2]}. \end{aligned}$$

2. F2:

$$F2(x,y) = \frac{1}{9}(\tanh(9y-9x)+1).$$

3. F3:

$$F3(x,y) = \frac{1.25+\cos(5.4y)}{6[1+(3x-1)^2]}.$$

The profiles of Franke's functions are shown in Figures 4.10, 4.11, and 4.12.

The numerical results for the Poisson and Helmholtz equations are listed in the Tables 4.7, and 4.8 respectively. The surface of these Franke's functions are more complex than those in previous examples. So, more Chebyshev nodes are needed to achieve high accuracy. While using the MFS, we choose a fictitious boundary which has the same shape as that of boundary. The sub-optimal source location for the source points (x_s, y_s) are found by using the LOOCV method for both boundary value problems. For the Poisson equation, the sub-optimal locations for $F1, F2$, and $F3$ are $1.449, 1.326$, and 1.382 respectively and

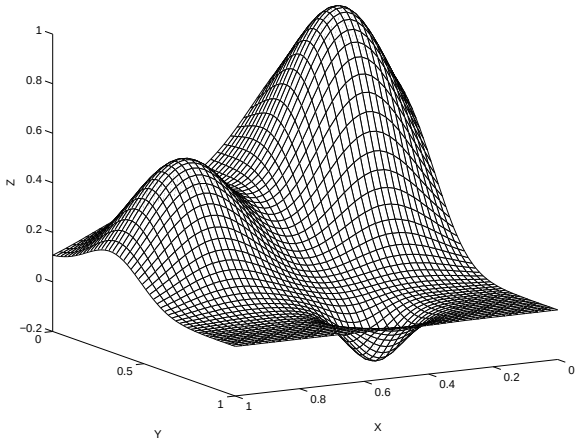

Figure 4.10: The profile of F1.

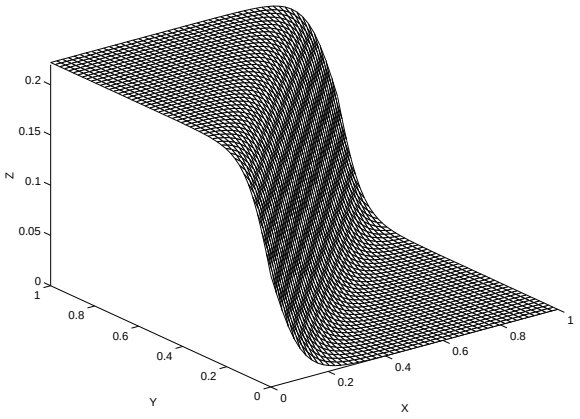

Figure 4.11: The profile of F2.

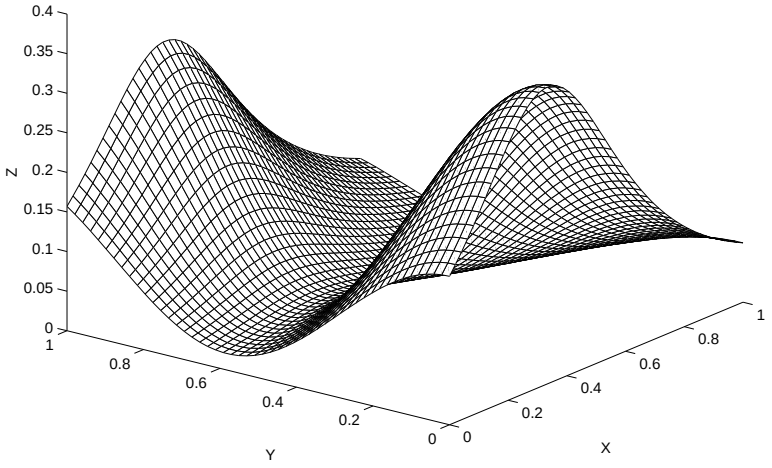

Figure 4.12: The profile of F3.

for the modified Helmholtz equation, they are $1.025, 1.024$, and 1.026 respectively. For the modified Helmholtz problem, the value of wave number λ directly affects the accuracy. We let $\lambda = 150$. The number of boundary points and test points taken are 396 and 64 respectively. The numerical results for the Poisson and the modified Helmholtz equations are listed in Tables 4.7 and 4.8 respectively. The error plots of the three Franke's test functions for the Poisson and the modified Helmholtz equations are given by the Figures 4.13 and 4.14 respectively.

Table 4.7: Example 7: MAE for Poisson using Franke's TFs.

Nx=Ny	MAE(F1)	MAE(F2)	MAE(F3)
10	9.823e-02	1.696e-02	5.437e-03
15	4.647e-03	1.196e-03	1.832e-05
20	1.147e-03	1.931e-04	6.534e-07
25	8.456e-05	4.516e-05	8.242e-08
30	6.414e-08	2.021e-06	1.011e-09
35	5.168e-09	6.367e-07	5.253e-11
40	2.113e-09	2.631e-08	3.724e-12
45	1.369e-10	1.928e-08	3.780e-12
50	5.240e-10	1.381e-09	3.077e-12

Table 4.8: Example 7: MAE for Helmholtz using Franke's TFs.

Nx=Ny	MAE(F1)	MAE(F2)	MAE(F3)
10	2.647e-02	1.196e-03	1.832e-03
15	9.943e-03	3.120e-04	3.866e-05
20	5.617e-04	2.182e-04	1.072e-06
25	8.868e-05	4.992e-05	7.900e-08
30	3.312e-06	2.158e-06	1.807e-09
35	6.488e-08	1.395e-06	5.202e-11
40	1.816e-09	1.192e-07	1.100e-12
45	5.836e-11	1.474e-08	6.361e-14
50	6.732e-13	8.710e-10	2.026e-15

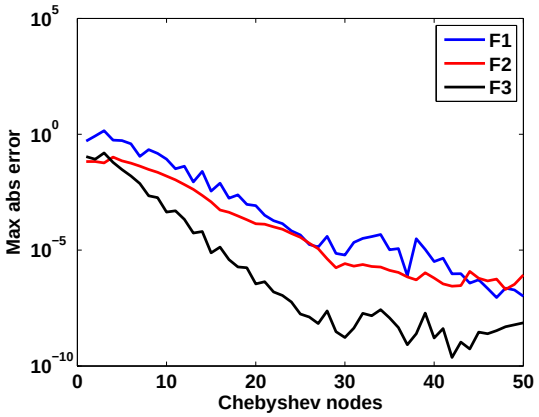

Figure 4.13: Error for Poisson on Franke's TFs.

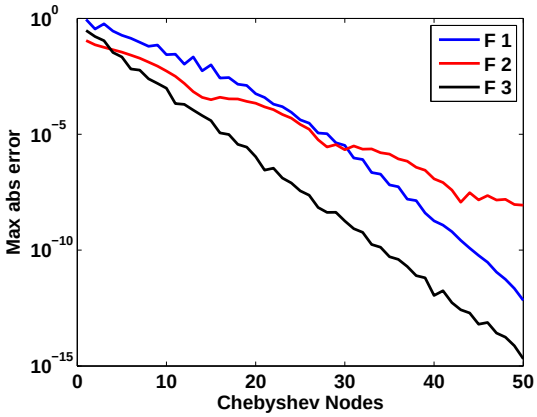

Figure 4.14: Error for Helmholtz on Franke's TFs.

4.1.8 Higher Order PDEs

In the previous examples, the second order PDEs including Poisson and modified Helmholtz equations are solved. In this example, following fourth order PDE with domain Ω being a

unit square is considered:

$$\begin{cases} (\Delta^2 - \lambda^4)u &= f(x,y), \quad (x,y) \in \Omega, \\ u &= g(x,y), \quad (x,y) \in \partial\Omega, \\ \Delta u &= h(x,y), \quad (x,y) \in \partial\Omega. \end{cases} \tag{4.4}$$

where $\lambda = 50$, f, g, and h are given functions such that the exact solution is

$$u(x,y) = \sin(\pi x)\cos\left(\frac{\pi y}{2}\right), \ \ (x,y) \in \Omega.$$

Since $\Delta^2 - \lambda^4 = (\Delta - \lambda^2)(\Delta + \lambda^2)$, we calculate the particular solution u_p of (4.4) in two steps,

$$(\Delta + \lambda^2)u_p = v_p, \tag{4.5}$$

$$(\Delta - \lambda^2)v_p = f. \tag{4.6}$$

Using Chebyshev polynomial, we can find v_p from (4.6) and then find u_p from (4.5). Hence, we don't have to take the derivatives of Chebyshev polynomial four times. We use 276 boundary points and 64 test points and the well-known LOOCV method is used to find the sub-optimal source radius r. In this case, a circle of radius 2.4 is chosen. From the Table 4.9, the high accuracy of our proposed method is observed. This shows that proposed method is equally applicable for solving other fourth order PDEs too.

Table 4.9: Example 8: MAE for 4th order PDE.

Nx=Ny	Max Abs Error
10	1.249e-05
12	3.968e-07
14	5.573e-09
16	7.300e-11
18	1.308e-12
20	1.554e-12
22	1.537e-12
24	8.236e-11
26	5.652e-10
28	4.093e-08
30	6.473e-08

4.2 HCPS using Collocation Trefftz Method

The MFS is a very powerful boundary method for solving homogeneous equations which requires fictitious boundary. Another boundary only method, which does not require

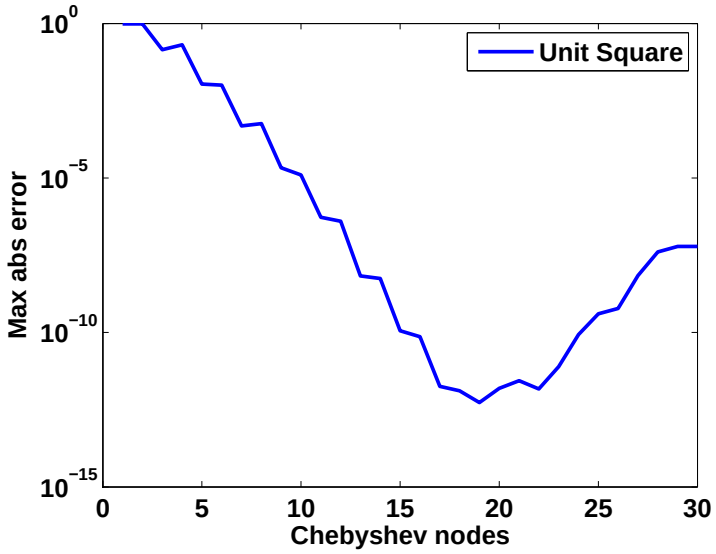

Figure 4.15: Error plot on fourth order PDE.

fictitious boundary, is Collocation Trefftz method (CTM) which is described in Section 2.3.2. The CTM avoids the determination of a suitable location for source points, which is a great advantage over the MFS. In the following numerical examples, Chebyshev polynomial is coupled with the CTM for solving Poisson equation and modified Helmholtz equation.

4.2.1 Poisson Equation

The governing equation is given by (4.1). As illustrated in 2.3.2, while using the CTM, T-complete functions are taken as a basis function. The list of T-complete functions is given in Table 4.3. By the direct implementation of the CTM, the resulting matrix is highly ill-conditioned. So care must be taken to overcome this difficulty while employing the CTM. In this dissertation, numerical experiments are performed by considering $N_1 \lneq N_b$, where N_1 is the order of the T-complete functions and N_b is the number of boundary points. This is due to the fact that $besseli(j, \lambda r)$ becomes very large for large j, which might affect the accuracy directly. Hence, for the numerical experiments, while implementing the CTM, the order of T-complete functions taken is 61. Similarly, boundary and test points taken are 250 and 120 respectively. The numerical result shown in Table 4.10 verifies that proposed hybrid Chebyshev polynomial scheme is highly accurate and stable.

4.2.2 Modified Helmholtz Equation

The governing equation is given by (4.2). For the CTM, the T-complete functions are listed in Table 4.3. We used wave number $\lambda = 35$. As usual 250 boundary points and 120 test

Table 4.10: Example 9: MAE for CTM in Poisson Equation.

Nx=Ny	Peanut	Star	Cassini	Amoeba
10	2.376e-04	8.963e-03	5.671e-05	4.604e-02
12	6.479e-06	3.583e-04	1.066e-06	3.227e-03
14	1.409e-07	2.186e-05	1.639e-08	1.524e-04
16	2.464e-09	5.455e-07	1.945e-10	4.482e-06
18	2.571e-11	1.809e-08	2.399e-12	1.749e-07
20	3.228e-13	3.036e-10	1.831e-14	3.916e-09
22	2.109e-15	5.547e-12	1.110e-15	8.989e-11
24	1.322e-15	6.872e-14	1.443e-15	9.743e-13
26	1.332e-15	2.331e-15	1.720e-15	1.887e-14
28	1.110e-15	2.567e-15	1.276e-15	6.022e-15
30	1.363e-13	2.356e-10	8.579e-11	5.020e-13

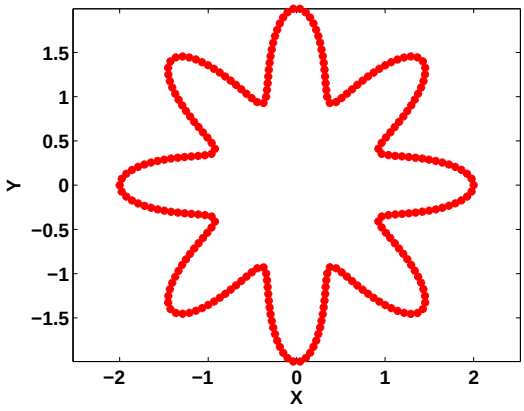

Figure 4.16: The profile of original domain.

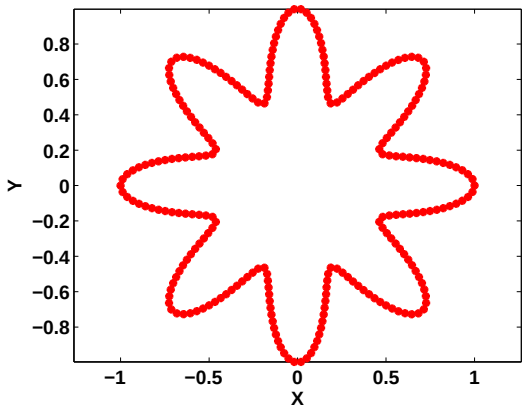

Figure 4.17: Transformed domain.

points are taken to verify the numerical accuracy. It can be inferred clearly that proposed method is highly accurate and efficient. The numerical result is given in Table 4.11. The computational domain is bounded by the cassini curve as shown in Figure **??**, which is defined by the following parametric equation:

$$\partial\Omega = \{(x,y)|x = \rho\cos\theta, y = \rho\sin\theta,\ 0 \le \theta \le 2\pi\},$$

where

$$\rho = \left(\cos(2\theta) + \sqrt{2 - \sin^2(2\theta)}\right)^{\frac{1}{2}}.$$

The error plot of Poisson equation and modified Helmholtz equation using the collocation Trefftz method (CTM) is given in the Figures 4.18 and 4.19 respectively.

Table 4.11: Example 10: MAE for CTM in modified Helmholtz.

Nx=Ny	Peanut	Cassini	Amoeba	Star
10	4.886e-05	3.569e-05	1.765e-02	3.338e-03
12	1.406e-06	3.561e-07	1.396e-03	1.930e-04
14	2.567e-08	1.229e-08	6.037e-05	7.078e-06
16	4.004e-10	3.995e-10	2.286e-06	2.205e-07
18	1.248e-11	3.040e-12	8.017e-08	4.462e-09
20	3.441e-13	5.784e-14	1.888e-09	1.039e-10
22	4.169e-15	6.952e-15	5.944e-11	2.002e-12
24	1.355e-14	2.638e-14	2.201e-12	5.018e-14
26	1.528e-14	4.560e-14	6.974e-14	1.998e-14
28	2.950e-14	8.115e-14	7.327e-15	2.048e-14
30	8.374e-14	7.387e-13	1.690e-14	1.328e-14

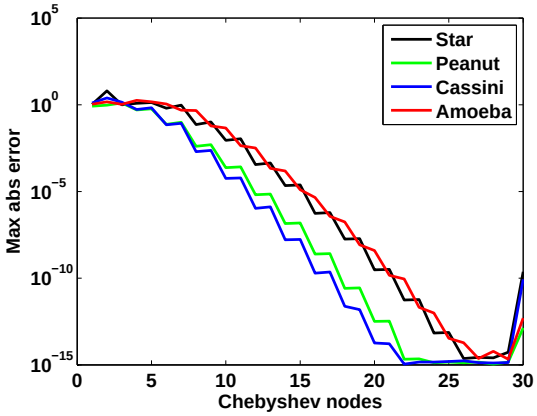

Figure 4.18: The profile of error plot for Poisson equation.

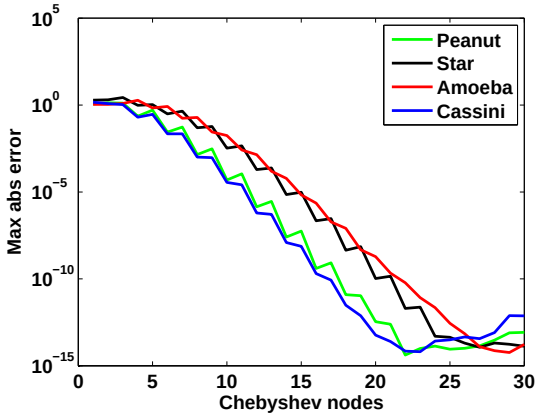

Figure 4.19: The profile of error plot for modified Helmholtz equation.

4.3 Comparison of the MFS and CTM

It is well-known fact that the MFS and the CTM are both boundary only meshless methods. Theoretically both methods are considered as the special case of Trefftz method (TM). The fundamental solution of differential operator is required for the MFS and source points are placed on the fictitious boundary to avoid the singularity. The CTM, on the other hand, does not require fictitious boundary but uses T-complete functions of the differential operator as a basis function. In this dissertation, we have compared the performance of the MFS and the CTM. The computational domains for the numerical examples are amoeba-shaped and cassini-shaped. The number of boundary points and test points taken are 250 and 120 respectively. We use the same number of source points and boundary points for the MFS. While implementing the CTM, the order of T-complete function taken for both examples

is 61. We let the wave number (λ) for the modified Helmholtz equation is 50. We observe highly accurate and stable solution in both examples. Numerical examples show that the performance of the CTM is in general better than the MFS.

4.3.1 The MFS and The CTM on Poisson Equation

Table 4.12 shows the numerical result on Poisson equation in various irregular domains using the MFS and the CTM. The error plot is given in Figure 4.20.

Table 4.12: Example 11: MAE for the MFS and CTM in Poisson.

	MFS		CTM	
Nx=Ny	Cassini	Amoeba	Cassini	Amoeba
10	1.640e-03	4.163e-02	5.671e-05	4.604e-02
12	4.034e-05	2.832e-03	1.066e-06	3.227e-03
14	9.067e-07	1.396e-04	1.639e-08	1.524e-04
16	1.199e-08	6.705e-06	1.945e-10	4.482e-06
18	1.601e-10	2.369e-07	2.399e-12	1.749e-07
20	1.210e-12	3.761e-09	1.831e-14	3.916e-09
22	8.099e-14	7.877e-11	1.110e-15	8.989e-11
24	1.922e-13	1.213e-12	1.443e-15	9.743e-13
26	1.842e-13	4.833e-13	1.720e-15	1.887e-14
28	6.796e-13	9.527e-13	1.276e-15	6.022e-15
30	1.523e-13	1.169e-12	8.579e-11	5.020e-13

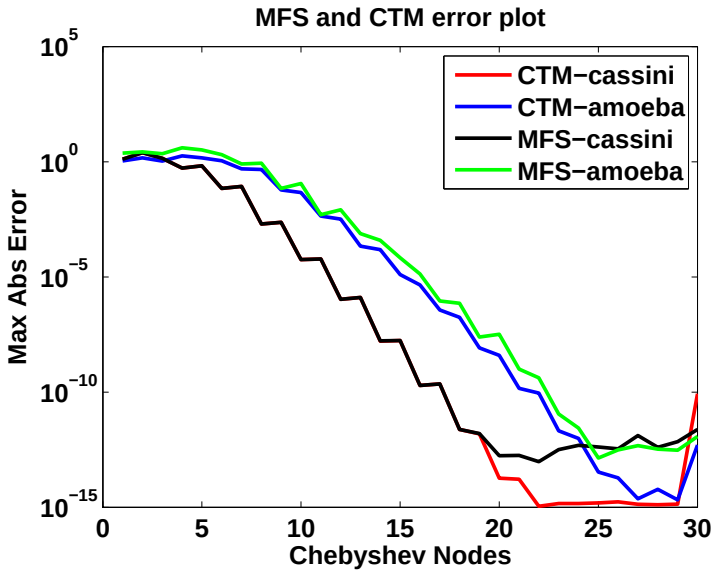

Figure 4.20: MAE for the Poisson Equation.

4.3.2 The MFS and CTM on Helmholtz Equation

Table 4.13 shows the numerical result on modified Helmholtz equation in various irregular domains using the MFS and CTM. The error plot is given in the Figure 4.21.

Table 4.13: Example 12: MAE for MFS and CTM in modified Helmholtz.

	MFS		CTM	
Nx=Ny	Amoeba	Star	Amoeba	Star
10	1.806e-02	3.199e-02	1.765e-02	3.338e-03
12	1.396e-03	2.401e-03	1.396e-03	1.930e-04
14	8.737e-05	1.269e-04	6.037e-05	7.078e-06
16	3.464e-06	5.005e-06	2.286e-06	2.205e-07
18	1.148e-07	1.530e-07	8.017e-08	4.462e-09
20	3.741e-09	3.736e-09	1.888e-09	1.039e-10
22	1.129e-10	7.452e-11	5.944e-11	2.002e-12
24	3.365e-12	1.238e-12	2.201e-12	5.018e-14
26	9.525e-14	1.820e-14	6.974e-14	1.998e-14
28	1.050e-13	2.231e-14	7.327e-15	2.048e-14
30	9.564e-14	2.907e-14	1.690e-14	1.328e-14

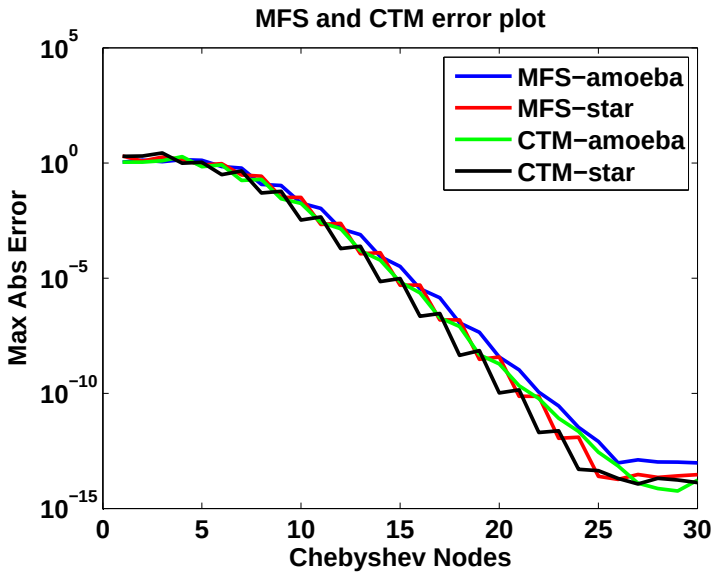

Figure 4.21: MAE for the modified Helmholtz equation.

We note that, by the direct implementation of the collocation Trefftz method, the resulting linear algebraic systems from both the Poisson and the modified Helmholtz equations are highly ill-conditioned. As discussed in Section 2.3.3, we use the multiple scales method to obtain the equilibrated matrix which provides an equivalent but less ill-conditioned linear

system. Comparison of the condition numbers between the conventional Trefftz method and the equilibrated Trefftz method on the Poisson equation and the modified Helmholtz equation over the amoeba-shaped domain are shown in the Figures 4.22 and 4.23 respectively. From the figures, we clearly notice that the condition number from the conventional Trefftz method grows rapidly as the order of the Trefftz method increases and the condition number from the equilibrated Trefftz method is much better and relatively stable.

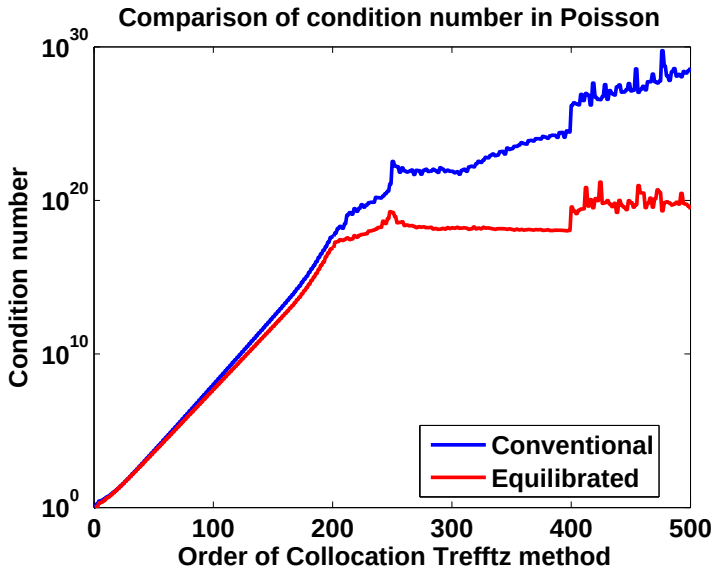

Figure 4.22: Comparison of condition numbers in Poisson equation.

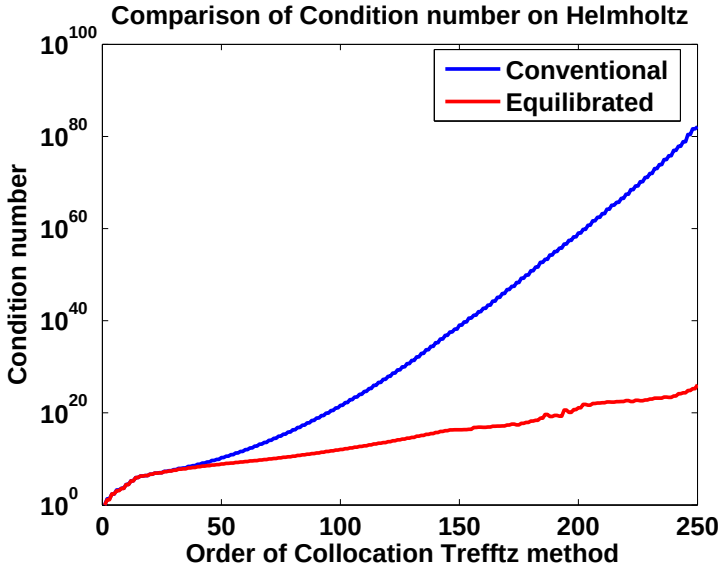

Figure 4.23: Comparison of condition numbers in modified Helmholtz equation.

Chapter 5

NUMERICAL RESULTS UTILIZING ONE-STEP HCPS

Various numerical examples in two dimensions (2D) and three dimenstions (3D) are presented to verify the accuracy of the one-step hybrid Chebyshev polynomial scheme (HCPS) in this section. The advantage of one-step HCPS over two-step HCPS is its applicability to solve PDEs with variable coefficients. Hence, four numerical examples on variable coefficients PDEs with Dirichlet and Neumann boundary conditions on the different irregular domains and the Cauchy-Navier equations for the displacements (u_1, u_2) on the unit square have been presented. We investigate applications of the one-step HCPS for the numerical solution of 3D boundary value problems in complex geometries governed by the Laplace equation and subject to Dirichlet boundary conditions. For the MFS, we use the well-known leave-one-out cross validation (LOOCV) algorithm to determine the sub-optimal source location of the fictitious boundary from the original boundary [56].

5.1 PDEs with Variable Coefficients

5.1.1 Example 1

We consider the following boundary value problem with a Dirichlet boundary condition:

$$\begin{aligned} \Delta u(x,y) - x^2 y u(x,y) &= f(x,y),\ (x,y) \in \Omega, \\ u(x,y) &= g(x,y),\ (x,y) \in \partial\Omega, \end{aligned} \tag{5.1}$$

where f, and g are chosen based on the following exact solution:

$$u(x,y) = \cos(3x) - \cos(3y).$$

Table 5.1 shows the numerical results for the amoeba-shaped, cassini-shaped, star-shaped, and unit square domains. We have used 250 boundary points and 120 test points for amoeba, star and cassini whereas 276 boundary points and 64 test points for the unit square. To avoid singularities when using the MFS, we distribute points on a circle of radius r. By using the LOOCV, the sub-optimal radii r for the cassini, star, amoeba, and the unit square are 1.698, 1.702, 2.201 and 1.505 respectively. Since Chebyshev polynomials provide spectral convergence on the domain and the MFS is also highly accurate boundary method, the l

solutions are highly accurate as expected. The numerical result clearly verifies this fact. The computational domain Ω as shown in Figure 5.1 is bounded by the curve defined by the following parametric equation:

$$\partial\Omega = \{(x,y)|x = \rho\cos\theta, y = \rho\sin\theta,\ 0 \le \theta \le 2\pi\},$$

where

$$\rho = e^{\sin(\theta)}\sin^2(2\theta) + e^{\cos(\theta)}\cos^2(2\theta).$$

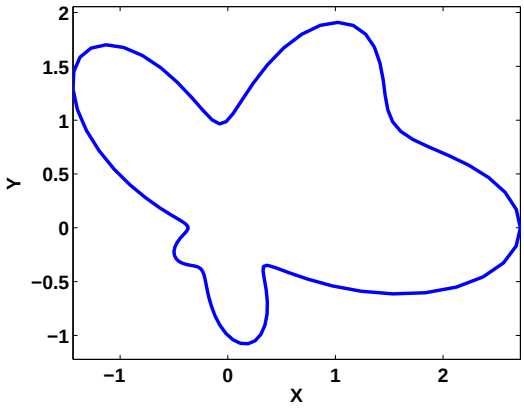

Figure 5.1: The profile of Ameoba domain.

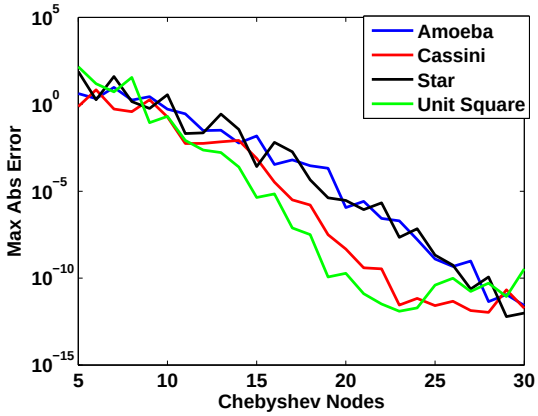

Figure 5.2: Error Plot of Example 1.

Table 5.1: Example 1: MAE using various Nx and Ny.

Nx=Ny	Unit square	Amoeba	Cassini	Star
10	4.400e-02	9.527e-01	6.717e-03	9.864e-01
12	5.545e-04	5.525e-01	2.186e-04	1.627e-02
14	1.400e-05	5.143e-02	3.449e-05	1.533e-03
16	5.683e-07	1.370e-03	5.897e-06	6.457e-03
18	1.695e-09	6.769e-04	2.029e-07	3.119e-05
20	5.590e-11	8.290e-05	1.343e-09	2.814e-06
22	3.269e-13	1.997e-06	1.091e-11	1.597e-07
24	5.464e-13	5.473e-08	8.548e-14	5.549e-09
26	1.556e-11	2.562e-09	1.751e-13	9.531e-11
28	5.709e-11	5.367e-11	5.986e-13	2.803e-12
30	6.344e-11	1.230e-12	1.900e-13	1.012e-12

5.1.2 Example 2

We consider the following mixed boundary value problem:

$$\begin{aligned} \Delta u(x,y) - x^2 y \frac{\partial u(x,y)}{\partial x} &= f(x,y),\ (x,y) \in \Omega, \\ u(x,y) &= g(x,y),\ \ (x,y) \in \partial\Omega, \\ \frac{\partial u(x,y)}{\partial \mathbf{n}} &= h(x,y),\ \ (x,y) \in \partial\Omega, \end{aligned} \tag{5.2}$$

where $\partial\Omega_1 \cup \partial\Omega_2 = \partial\Omega$ and $\partial\Omega_1 \cap \partial\Omega_2 = \emptyset$, f, g, and h are given functions based on the analytical solution:

$$u(x,y) = \sin(\pi x)\cos\left(\frac{\pi y}{2}\right).$$

The computational domain is bounded by the Cassini curve as shown in Figure 5.3, which is defined by the following parametric equation:

$$\partial\Omega = \{(x,y) | x = \rho\cos\theta, y = \rho\sin\theta, 0 \le \theta \le 2\pi\},$$

where

$$\rho = \left(\cos(3\theta) + \sqrt{2 - \sin^2(3\theta)}\right)^{\frac{1}{3}}.$$

In this example, we consider the amoeba-shaped, cassini-shaped, and the unit square domains. In the numerical experiments, we chose 250 uniformly distributed boundary points and 120 randomly distributed test points for amoeba-shaped and cassini-shaped domains, whereas 276 boundary points and 64 test points for unit square. We let the source points distribute on a circle of radius r. We used the LOOCV method to choose the sub-optimal source radius which are as follows: 2.25 for amoeba, 1.98 for cassini, and 2.01 for the unit square. From Table 5.2, we can clearly see that the proposed method is highly accurate and stable.

5.1.3 Example 3

In this example, we consider the following modified Helmholtz equation with Dirichlet boundary condition:

$$\begin{aligned} (\Delta - \lambda^2) u(x,y) &= f(x,y),\ \ (x,y) \in \Omega, \\ u(x,y) &= g(x,y),\ \ (x,y) \in \partial\Omega, \end{aligned} \tag{5.3}$$

where $f(x,y)$, and $g(x,y)$ are generated from the following analytical solution:

$$u(x,y) = \cos(3x) - \cos(3y).$$

Table 5.2: Example 2: MAE for mixed boundary condition.

Nx=Ny	Unit Square	Cassini	Amoeba
10	4.166e-06	6.710e-04	4.430e-02
12	2.758e-08	1.088e-05	7.188e-03
14	3.915e-10	3.589e-07	2.700e-03
16	2.286e-12	6.217e-08	2.683e-04
18	1.232e-12	1.549e-10	1.375e-06
20	2.550e-15	5.339e-12	2.764e-08
22	9.992e-16	1.150e-13	1.325e-09
24	1.221e-15	2.790e-15	7.825e-11
26	1.663e-15	6.754e-15	2.443e-13
28	1.223e-15	2.746e-15	7.340e-15
30	2.381e-15	2.162e-15	1.469e-14

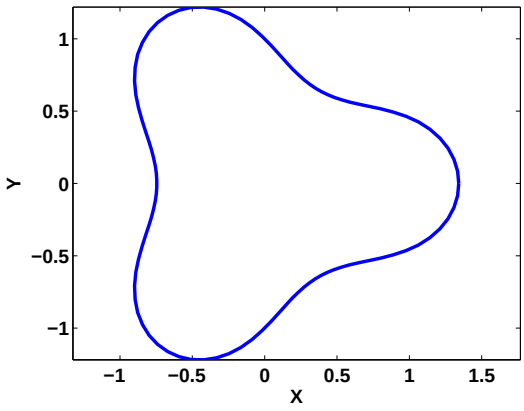

Figure 5.3: The profile of Cassini domain.

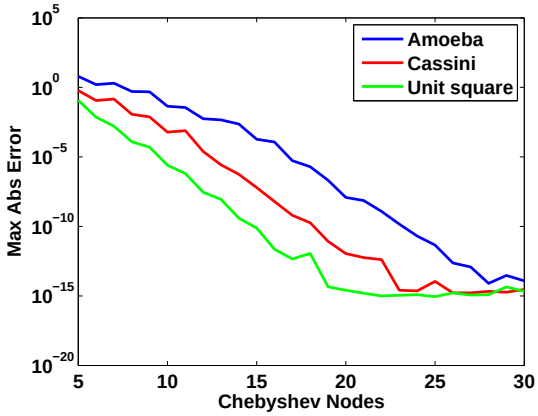

Figure 5.4: Error Plot of Example 2.

The computational domain Ω as shown in Figure 5.5 is bounded by the curve defined by the following parametric equation:

$$\partial\Omega = \{(x,y)|x = \rho\cos\theta, y = \rho\sin\theta, 0 \leq \theta \leq 2\pi\},$$

where

$$\rho = 1 + \cos^2(4\theta).$$

Table 5.3 shows the numerical result for the modified Helmholtz equation in different domains: amoeba-shaped, cassini-shaped and star-shaped domains. For the MFS, the fictitious boundary (x_s, y_s) where the source points are located is chosen to have the same shape as that of the boundary. The sub-optimal source location in this case is found by using well-known LOOCV algorithm. The sub-optimal source location for amoeba-shaped, cassini-shaped and star-shaped domains are 1.009, 1.015, and 1.016 respectively. The

number of boundary and test points taken for the amoeba, cassini and star domains are 250 and 120 respectively whereas for the unit square, 276 and 64 respectively. The wave number $\lambda = 35$ is chosen for the numerical results. From the numerical results, we can easily see that our method is highly accurate and stable.

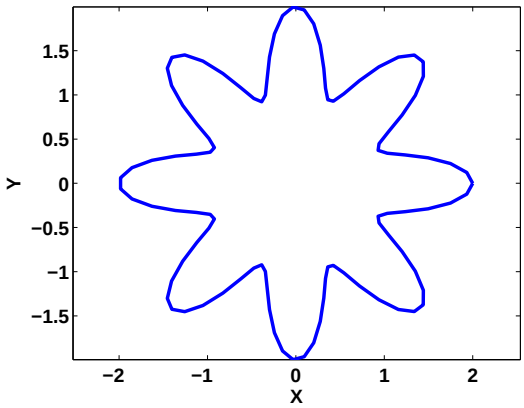

Figure 5.5: The profile of Star-shaped domain.

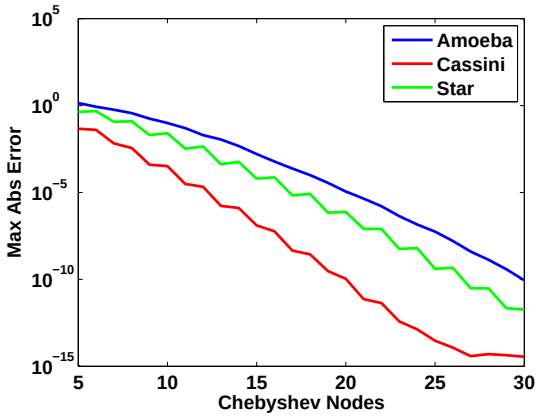

Figure 5.6: Error Plot of Example 3.

Table 5.3: Example 3: MAE for modified Helmholtz problem.

Nx=Ny	Cassini	Amoeba	Star
10	4.711e-04	8.765e-02	3.179e-02
12	1.288e-05	1.396e-02	2.375e-03
14	2.546e-06	8.609e-03	1.249e-04
16	3.938e-08	3.742e-04	4.897e-05
18	4.311e-09	1.632e-05	1.488e-06
20	4.872e-10	7.067e-06	3.607e-07
22	4.920e-12	2.793e-07	8.051e-08
24	3.219e-13	1.008e-08	1.313e-09
26	1.548e-14	3.288e-09	5.151e-10
28	5.922e-15	1.801e-09	1.398e-11
30	3.103e-15	5.750e-10	2.386e-12

5.1.4 Example 4

In this example, we consider the following boundary value problem in a gear-shaped domain:

$$\begin{aligned} \Delta u(x,y) - x^2 y u(x,y) &= f(x,y),\ (x,y) \in \Omega, \\ u(x,y) &= g(x,y),\ (x,y) \in \partial\Omega, \end{aligned} \tag{5.4}$$

where f, and g are given functions based on the following exact solution

$$u(x,y) = \cos(3x) - \cos(3y).$$

The computational domain Ω in this example is a gear-shaped domain as shown in Fig 5.7 which is bounded by the following parametric equation:

$$\partial\Omega = \left\{ (x,y) | x = \rho(t)\cos\left(t + \frac{1}{2}\sin(7t)\right), y = \rho(t)\sin\left(t + \frac{1}{2}\sin(7t)\right),\ 0 \le \theta < 2\pi \right\},$$

where

$$\rho(t) = \frac{1}{2}\left(t + \frac{1}{2}\sin(7t)\right).$$

Source points are placed on a circle of radius r when using the MFS. By using the well-known LOOCV, the sub-optimal value of r in this case is 1.6. For the numerical implementation, 300 uniformly distributed points on the boundary are taken. Table 5.4 shows the maximum absolute errors for various Chebyshev nodes. Our numerical scheme is highly accurate and stable in this case too.

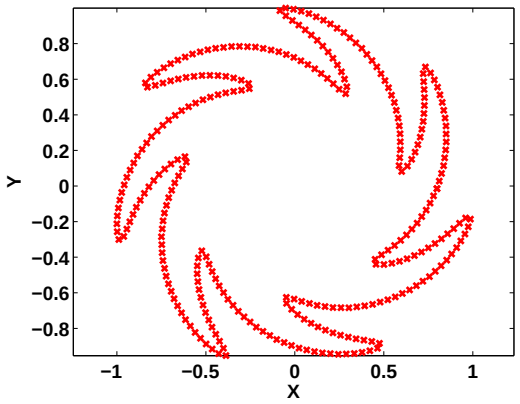

Figure 5.7: The profile of gear shape.

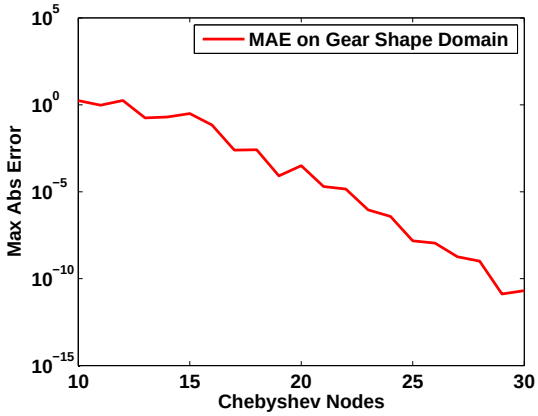

Figure 5.8: Error Plot on gear-shaped domain.

5.2 Cauchy-Navier Equations of Elasticity

Finally, to verify the effectiveness of our proposed numerical scheme HCPS using one-step approach, we consider a system of equations given by (3.35)-(3.36) known as Cauchy-Navier equations of elasticity subject to the Dirichlet boundary conditions [30]. In this example $f_1, f_2, g_1,$ and h_1 are given functions based on the following exact solution:

$$u_1(x,y) = e^{x+y},\ \ u_2(x,y) = \sin(x+y).$$

Table 5.4: Example 4: MAE on gear shape domain.

Nx=Ny	Maximum Abs Error
10	1.754e+00
12	1.781e+00
14	2.011e-01
16	6.898e-02
18	2.611e-03
20	3.171e-04
22	1.426e-05
25	3.809e-07
26	1.098e-08
28	1.023e-09
30	2.032e-11

We take Poisson's ratio and the shear modulus to be $\nu = 0.3$, and $\mu = 1$ respectively. Table 5.5 shows the maximum absolute errors in u_1 and u_2 for various Chebyshev nodes. From the numerical results, we conclude that our numerical scheme is equally applicable to the Cauchy-Navier equations too.

Table 5.5: MAE for Cauchy-Navier Equation.

Nx=Ny	MAE (u_1)	MAE (u_2)
10	5.423e-06	8.814e-07
11	4.763e-07	3.319e-07
12	3.224e-08	1.552e-08
13	4.607e-09	4.964e-09
14	1.113e-09	3.111e-10
15	3.966e-11	5.788e-11
16	5.803e-12	1.494e-11
17	1.088e-10	1.497e-10
18	2.923e-10	3.688e-10
19	4.244e-10	2.831e-10
20	9.320e-10	1.121e-09

5.3 3D Boundary Value Problems

HCPS was proven to be highly accurate, easy to implement, and very efficient numerical method for solving 2D boundary value problems. It is a challenging task to work in higher dimensions with complex geometries and large scale problems. However, it is relatively easy to work in 3D problems in meshless method as compared to the mesh based methods such

as finite element and finite difference method [4, 51, 55]. The hybrid formulation in three dimensional space would be pretty much similar as that of two dimensional formulation. So readers are referred to Section 3.3.2 for more details. Various numerical examples on 3D domains are presented in this section.

In our numerical experiments, to verify the effectiveness of the one-step hybrid Chebyshev polynomial scheme (HCPS), we consider different three-dimensional domains such as 3D Stanford Bunny, unit sphere, double-sphere, and bumpy-sphere as shown in Figures 5.9, 5.10, 5.11, and 5.12 respectively.

Let us consider the following three dimensional boundary value problem:

$$\mathcal{L}u(x,y,z) = f(x,y,z), \;\; (x,y,z) \in \Omega, \tag{5.5}$$

with Dirichlet boundary condition

$$u(x,y,z) = g(x,y,z), \;\; (x,y,z) \in \partial\Omega_1, \tag{5.6}$$

and Neumann boundary condition

$$\frac{\partial u(x,y,z)}{\partial \mathbf{n}} = h(x,y,z), \;\; (x,y,z) \in \partial\Omega_2, \tag{5.7}$$

where $\Omega \subset \mathbb{R}^3$ is a simply connected domain bounded by a simple closed curve $\partial\Omega$, Ω_1 and Ω_2 are part of the boundary Ω with $\partial\Omega_1 \cup \partial\Omega_2 = \Omega$, $\partial\Omega_1 \cap \Omega_2 = \emptyset$, $\mathcal{L}$ is an elliptic differential operator, f, g, and h are given functions.

5.3.1 3D Stanford Bunny

We first consider a Poisson equation with a Dirichlet boundary condition:

$$\begin{aligned} \Delta u(x,y,z) &= f(x,y,z), \quad (x,y,z) \in \Omega, \\ u(x,y,z) &= g(x,y,z), \quad (x,y,z) \in \partial\Omega. \end{aligned} \tag{5.8}$$

The forcing term $f(x,y,z)$ and the boundary data $g(x,y,z)$ are given such that the exact solution is:

$$u(x,y,z) = \cos(x)\cos(y)\cos(z).$$

In this numerical experiment, our computational domain is the Stanford Bunny (see Figure 5.9) whose boundary data points are available at the website of the Stanford Computer Graphics Laboratory [1]. While implementing our numerical scheme, we use two different data sets of Stanford Bunny. The number of data points taken are 1889 and 8171 for the numerical experiment. First, we use regular size of Stanford bunny without blow up. N

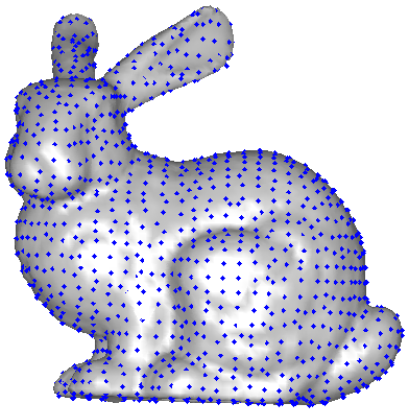

Figure 5.9: Profile of the Stanford Bunny with 1889 boundary points.

represents the total number of Chebyshev points taken for the numerical experiments. For the MFS, the fictitious boundary (x_s, y_s) where the source points are located is chosen to be the sphere. We use the LOOCV method to find the sub-optimal source radius which is 2.450 and 2.785 for the 8171 and 1889 data sets Stanford Bunny respectively. Table 5.6 shows the numerical result. We clearly see that our proposed method is highly accurate and stable for the three-dimensional Poisson equation.

Table 5.6: Max Abs Error for Stanford Bunny (Normal data).

N	1889 data	CPU(s)	8171 data	CPU(s)
1000	1.067e-05	0.42	5.540e-07	7.45
1728	3.761e-06	0.57	7.572e-06	9.34
2744	8.910e-07	0.90	1.082e-07	14.88
4096	7.222e-08	1.91	3.027e-09	15.04
5832	7.698e-10	5.04	1.165e-09	19.43
8000	4.215e-10	6.31	3.959e-10	37.73
10648	4.794e-11	16.90	5.309e-11	70.41
13824	1.702e-11	34.59	8.298e-11	99.20
17576	1.504e-11	66.87	3.666e-11	183.75
21952	5.881e-12	146.17	2.088e-11	332.89
27000	2.505e-11	241.17	5.233e-12	728.32

Usually the normal size (given data points) of standard Stanford bunny is very small. So, in this case, the coordinate of the boundary points are multiplied by 10 and use that data points for our numerical experiment. Table 5.7 demonstrates the numerical result for the blow up case. As usual, sphere is used for the fictitious boundary and the well-known

LOOCV method is used to find the sub-optimal source radius. The sub-optimal source radii are 2.510 and 2.750 for the 8171 and 1889 data sets respectively. Our numerical scheme performs better in the normal size than in the blow up case.

Table 5.7: Max Abs Error for Stanford Bunny (10 times blow up).

N	1889 data	CPU(s)	8171 data	CPU(s)
1000	1.987e+04	0.37	2.486e+03	8.99
1728	4.464e+01	0.78	3.790e+00	12.34
2744	1.204e-04	1.25	2.665e-04	13.83
4096	8.191e-06	1.91	6.674e-06	18.66
5832	1.263e-06	3.42	4.241e-07	27.43
8000	1.155e-07	6.61	1.720e-08	35.44
10648	5.178e-09	14.10	5.004e-09	77.96
13824	9.746e-10	31.27	2.508e-09	90.53
17576	4.205e-10	64.07	9.189e-10	178.97
21952	1.569e-10	134.51	8.535e-11	385.63
27000	5.734e-11	242.25	1.788e-11	691.18

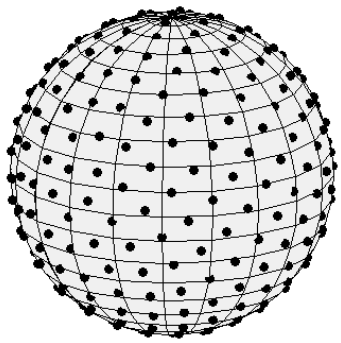

Figure 5.10: The computational Domain and the distributions of the boundary points on the surface of 3D sphere.

5.3.2 Sphere, Double Sphere and Bumpy Sphere

In this example, our 3D computational domains are unit sphere (see Figure 5.10), double-sphere (see Figure 5.11), and bumpy-sphere (see Figure 5.12). We consider Poisson equation (5.8) with Dirichlet boundary condition. For the MFS, the fictitious boundary where the source points are located is chosen to be Sphere. For our numerical experiment, the number of boundary points and test points taken for the sphere are 1000 and 360 respectively. Similarly for the double-sphere, boundary points and test points are 1000 and 416 respectively,

and for the bumpy-sphere 1000 and 120 respectively. We use the LOOCV method to find the sub-optimal source radius. The source radii r for sphere, double-sphere, and bumpy-sphere are 2.524, 3.013, and 3.854 respectively. We observe the numerical result in Table 5.8. From this observation, we assert that our numerical scheme is highly accurate, and efficient for three-dimensional boundary value problems.

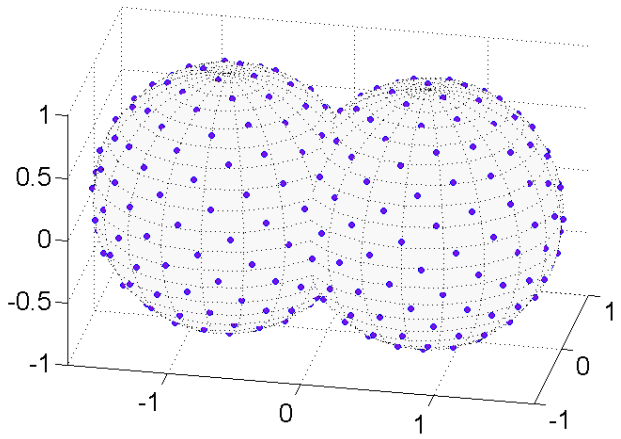

Figure 5.11: The computational Domain and the distributions of the boundary points on the surface of double-sphere.

Table 5.8: MAE for bumpy-sphere, sphere, and double-sphere.

N	Bumpy-sphere	CPU(s)	Sphere	CPU(s)	Double-sphere	CPU(s)
1000	3.549e-06	0.55	2.617e-06	0.50	4.617e-04	0.50
1331	8.834e-06	0.68	2.072e-06	0.70	3.581e-04	0.71
1728	1.315e-11	0.96	1.538e-11	1.03	8.103e-08	0.93
2197	1.112e-10	1.48	4.691e-11	1.42	4.973e-07	1.44
2744	2.318e-11	2.14	9.009e-11	2.17	8.827e-11	2.25
3375	1.040e-10	3.25	1.122e-11	3.72	1.396e-10	3.17
4096	5.414e-10	5.38	3.136e-11	5.06	1.961e-11	4.87
4913	4.294e-12	7.39	8.089e-11	7.69	2.328e-10	7.89
5832	5.126e-11	11.87	1.186e-10	11.78	1.004e-10	11.80
6859	1.600e-11	17.43	1.272e-11	17.57	1.163e-09	16.96
8000	7.867e-11	26.24	7.268e-11	25.72	5.347e-10	27.38

5.4 One-step HCPS with Constant Coefficient PDEs

In the Chapter 4, we employed two-step HCPS to solve various elliptic PDEs with constant coefficients. On the other hand, one-step HCPS is employed to solve a large class of

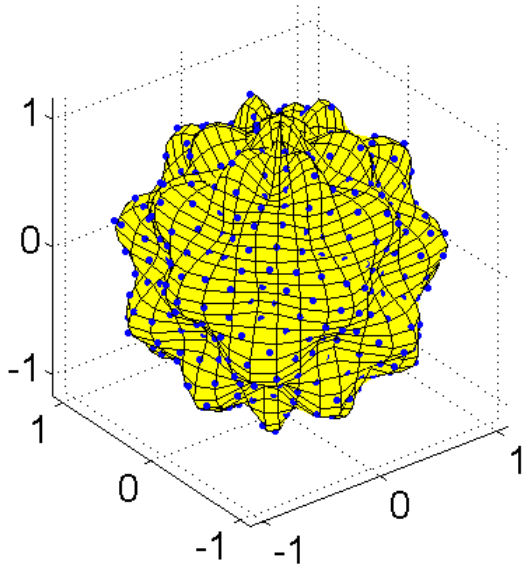

Figure 5.12: The computational domain of a bumpy-sphere and the distributions of the boundary points on the surface of the bumpy-sphere.

PDEs including variable coefficients. The performance of one-step HCPS on constant coefficients is also of particular interest. So, in this section, we explore the performance of one-step HCPS on constant coefficient PDEs. First, we consider the Poisson equation with Dirichlet boundary conditions (4.1) where $f(x,y)$, and $g(x,y)$ are generated from the following analytical solution:

$$u(x,y) = \cos(3x) - \cos(3y).$$

Table 5.9 shows the numerical results for the amoeba-shaped, cassini-shaped, and star-shaped domains. We used 250 boundary points and 120 test points for amoeba, star, and cassini as usual. To avoid singularities when using the MFS, we distribute source points on a circle of radius r outside the domain. By using the LOOCV method, the sub-optimal source radii r for the cassini-shaped, star-shaped, and amoeba-shaped domains are 1.998, 1.502, and 1.492 respectively.

To demonstrate the applicability of one-step HCPS for solving PDEs with constant coefficients, numerical experiment is performed in modified Helmholtz equation with the same analytical solution as above in different irregular domains. Table 5.10 presents the numerical result. For the MFS, the fictitious boundary where the source points are located is chosen to have the same shape as that of the original boundary. The sub-optimal source location is determined by the LOOCV which are 1.015, 1.023, and 1.034 for amoeba-shaped,

Table 5.9: Maximum Absolute Error for Poisson Equation.

Nx=Ny	Star	Amoeba	Cassini
10	4.252e-01	1.075e-01	2.029e-01
12	6.268e-03	1.767e-02	40118e-03
14	3.466e-04	2.507e-03	3.409e-04
16	5.138e-06	4.270e-04	1.162e-06
18	4.311e-07	1.006e-06	1.488e-08
20	6.482e-09	1.672e-08	3.607e-10
22	4.920e-10	3.536e-10	8.051e-11
24	5.902e-11	1.708e-11	2.363e-12
26	6.843e-12	4.298e-12	1.541e-12
28	1.722e-12	1.381e-12	7.308e-12
30	3.213e-111	5.269e-11	3.326e-11

Cassini-shaped and star-shaped domains respectively.

Table 5.10: Example 3: MAE for modified Helmholtz problem.

Nx=Ny	Cassini	Amoeba	Star
10	4.711e-04	8.765e-02	3.179e-02
12	1.288e-05	1.396e-02	2.375e-03
14	2.546e-06	8.609e-03	1.249e-04
16	3.938e-08	3.742e-04	4.897e-05
18	4.311e-09	1.632e-05	1.488e-06
20	4.872e-10	7.067e-06	3.607e-07
22	4.920e-12	2.793e-07	8.051e-08
24	3.219e-13	1.008e-08	1.313e-09
26	1.548e-14	3.288e-09	5.151e-10
28	5.922e-15	1.801e-09	1.398e-11
30	3.103e-15	5.750e-10	2.386e-12

From the numerical results as shown in Tables 5.9, and 5.10, we conclude that one-step HCPS is also applicable to PDEs with constant coefficients. The accuracy of one-step HCPS for solving PDEs with constant coefficients is similar to the two-step HCPS.

5.5 Chebyshev Collocation Methods versus RBF Collocation Methods

The Kansa method [32, 33] is considered as an effective global RBF collocation method in the meshless literature capable of solving various partial differential equations (PDEs). Chen *et al.* [6, 7] proposed new globalized version of the method of particular solution (MPS). After the notable development in this field for more than two decades, recently Monroe

[50] employed one-stage MFS-MPS hybrid method to solve elliptic PDEs with variable coefficients. All of these afore mentioned numerical scheme used radial basis functions (Table 2.1) as a basis function. In this dissertation, we propose hybrid Chebyshev polynomial scheme (HCPS) which utilize the Chebyshev collocation technique in which Chebyshev polynomials are used as a basis function. In this section, we compare the performance of our proposed numerical scheme HCPS with the RBF collocation methods such as the MPS and one-stage MFS-MPS method. For the uniformity and consistency on the numerical experiments, we have used 250 boundary points and 120 test points. Computational domain is cassini-shaped domain with 374 interior points for the RBF collocation methods. While using Chebyshev collocation method, the numerical accuracy is measured at different Chebyshev nodes 14, 20, and 26. For the numerical experiment of one-step HCPS, MPS, and MFS-MPS, we consider the boundary value problem (5.1) where $f(x,y)$, and $g(x,y)$ are generated from the following analytical solution:

$$u(x,y) = y\sin(\pi x) + x\cos(\pi y).$$

Table 5.11 shows the numerical results for the one-step HCPS and MPS. While implementing MPS, we used Gaussian, MQ, and IMQ RBFs as a basis function. Next, we

Table 5.11: Comparison of HCPS and RBF Collocation Methods for Eq. (5.1).

One-step HCPS	Cheby-nodes	Max Abs Error
	14	3.449e-05
	20	1.343e-09
	26	1.752e-13
MPS	RBFs	Max Abs Error
	Gaussian	1.468e-06
	MQ	2.740e-05
	IMQ	4.456e-06

present the numerical result for the modified Helmholtz equation with Dirichlet boundary condition for one-stage MFS-MPS scheme (Table 5.12). For this numerical experiment, 325 interior points, 250 boundary points and 120 test points are used for cassini-shaped domain while utilizing one-stage MFS-MPS. Multiquadrics, inverse multiquadrics, and r^7 radial basis function are used in this case. The well-known LOOCV method is used to find the sub-optimal shape parameter and source location.

In this last section, our goal is to compare the performance of hybrid Chebyshev polynomial scheme (HCPS) over the radial basis function collocation methods. From the numerical results of Table 5.11, we can easily observe that accuracy of three RBFs are almost same.

Table 5.12: Comparison of HCPS and RBF Collocation Methods for modified Helmholtz equation.

One-step HCPS	Cheby-nodes	Max Abs Error
	14	2.546e-06
	20	4.872e-10
	26	1.548e-14
MFS-MPS	RBFs	Max Abs Error
	r^7	7.897e-07
	MQ	3.260e-07
	IMQ	2.272e-06

However, when compared to one-step HCPS, the highest numerical accuracy of RBFCM is achieved in a less number of Chebyshev nodes. As the number of Chebyshev nodes increases, HCPS is far superior than the RBF collocation methods. Similar kind of conclusion can be drawn from the numerical result utilizing modified Helmholtz equation as shown in Table 5.12. Similar results have been obtained for various differential equations. The performance of one-step HCPS has proven to be superior than the MFS-MPS in term of accuracy. However, one drawback of the one-step HCPS is that the Chebyshev interpolation points need to extend to outside the domain which is not applicable for some problems.

Chapter 6

SOLVING FOURTH ORDER PDES USING RADIAL BASIS FUNCTION COLLOCATION METHOD

6.1 Introduction

Radial basis functions (RBFs) have played an important role for solving various partial differential equations (PDEs) that arise in the field of science and engineering for more than two decades. The main considerations for solving PDEs are accuracy, stability, efficiency and simplicity. To fulfill these criteria, Edward Kansa [32, 33], developed the radial basis function collocation method (RBFCM) which is known as the Kansa method. The Kansa method has been successfully applied to solve many challenging problems in science and engineering. Followed by several developments of meshless methods Chen *et al.* [6, 7] proposed a new method called the method of approximate particular solutions (MAPS) which uses the particular solution of RBFs to approximate the differential equation. The main disadvantages of the RBF collocation method is related to the formation of full and dense matrices that are very sensitive to the choice of the free shape parameter and the difficulty in solving problems with a large number of unknowns. This is due to the use of the radial basis function interpolation which increases the condition numbers of the related matrices as the number of nodes increases. Many RBF collocation methods have been developed to address the issues related to full, dense, and ill-conditioned matrices arising from the global RBF collocation method. To mitigate the computational cost for large-scale problems, Mai-Duy *et al.* [45] employed the domain decomposition method. In 2002, Chen *et al.* [8] proposed a multi-grid approach using compactly supported RBFs. In recent years, the localized version of RBF collocation methods such as the local Kansa method (LKM) and the localized method of approximate particular solutions (LMAPS)[58, 66] have been developed and widely used for solving large-scale problems. The main advantage of the local version of the RBF collocation methods is the collocation on subdomains which drastically reduces the collocation matrix size. These new methods are equally capable to compete with the traditional mesh-based numerical methods, such as finite element and finite difference methods.

Fourth order partial differential equations (PDEs) have a wide range of applications in various fields of science and engineering. Some examples of physical flows and engineering

problems modeled by fourth order PDEs are ice formation [52], fluids on lungs [29], image processing for noise removal [44], etc. Yao *et al.* [67] compared three meshless methods LMAPS, local direct RBF collocation method (LDRBFCM), and local indirect RBF collocation method (LIRBFCM) for solving heat diffusion equations. In [67], authors concluded that LMAPS and LIRBFCM had slightly better results. In this chapter, we focus on RBF collocation methods for solving fourth-order PDEs in both global and local cases. First, we use the Kansa method and the method of approximate particular solutions using multiquadric (MQ) and inverse multiquadric (NMQ) radial basis functions. Here, we note that the corresponding differentiations and integrations are required to obtain closed form particular solutions of RBFs. Next, we employ the new approach for solving fourth-order PDEs both locally and globally. Finally, direct RBFCMs and new RBFCMs are compared for the approximation of functions.

6.2 Governing Equations

We consider a fourth-order PDE defined on a fixed domain Ω with boundary $\partial\Omega$ in 2D,

$$\mathcal{L}u(x,y) = f(x,y), \ \ (x,y) \in \Omega, \tag{6.1}$$

Dirichlet boundary condition

$$u(x,y) = g(x,y), \ \ (x,y) \in \partial\Omega, \tag{6.2}$$

Neumann boundary condition

$$\frac{\partial u(x,y)}{\partial \mathbf{n}} = h(x,y), \ \ (x,y) \in \partial\Omega, \tag{6.3}$$

where

$$\mathcal{L} = \Delta^2 + \alpha(x,y)\frac{\partial}{\partial x} + \beta(x,y)\frac{\partial}{\partial y} + \gamma(x,y),$$

Δ^2 denotes the biharmonic operator, Δ denotes the Laplace operator, $\partial/\partial\mathbf{n}$ is the normal derivatives on the boundary $\partial\Omega$, and α, β, γ, f, g, h are given functions.

6.3 New Formulation for Fourth-order PDEs

In this approach, the formulation of the problem starts with the representation of $\Delta u = w$, then (6.1)–(6.3) will be reduced to the following system of equations:

$$\Delta w(x,y) + \mathcal{L}u(x,y) = f(x,y), \ \ (x,y) \in \Omega, \tag{6.4}$$

$$w - \Delta u = 0, \;\; (x,y) \in \Omega, \tag{6.5}$$

where

$$\mathcal{L} = \alpha(x,y)\frac{\partial}{\partial x} + \beta(x,y)\frac{\partial}{\partial y} + \gamma(x,y),$$

Dirichlet boundary condition

$$u(x,y) = g_1(x,y), \;\; (x,y) \in \partial\Omega, \tag{6.6}$$

Neumann boundary condition

$$\frac{\partial u(x,y)}{\partial \mathbf{n}} = g_2(x,y), \;\; (x,y) \in \partial\Omega, \tag{6.7}$$

where $u(x,y)$, g_1, and g_2 are known. Let $u = \psi(r)$ be a radial basis function, then $\Delta u = \phi$.

The important part of this formulation involves the approximation of the solutions u and w with a linear combination of RBFs as shown below:

$$\begin{aligned} \hat{u}(x) &= \sum_{i=1}^{N} a_i \psi(\|x - x_i\|), \\ \hat{w}(x) &= \sum_{i=1}^{N} b_i \psi(\|x - x_i\|), \end{aligned}$$

where $\{a_i\}_{i=1}^N$ and $\{b_i\}_{i=1}^N$ are coefficients to be determined. The above solutions u and w can be written as $\hat{u} = [\psi][a]$ and $\hat{w} = [\psi][b]$ which leads to $[a] = [\psi]^{-1}\hat{u}$ and $[b] = [\psi]^{-1}\hat{w}$. So then, (6.4)-(6.7) reduce respectively to the following equations:

$$\left[\alpha(x,y)\left[\frac{\partial \psi}{\partial x}\right][\psi^{-1}] + \beta(x,y)\left[\frac{\partial \psi}{\partial y}\right][\psi^{-1}] + \gamma(x,y)\right]\hat{u} + [\phi][\psi^{-1}]\hat{w} = f, \tag{6.8}$$

$$[\phi][\psi^{-1}]\hat{u} - \hat{w} = 0, \tag{6.9}$$

$$\hat{u} = g_1, \tag{6.10}$$

$$\left[\frac{\partial \psi}{\partial x}\right][\psi^{-1}]n_x + \left[\frac{\partial \psi}{\partial y}\right][\psi^{-1}]n_y = g_2. \tag{6.11}$$

Finally, we solve the above block matrix system to determine the unknown coefficients $\{a_i\}$ and $\{b_i\}$. Here, we observe that the size of this block matrix will be twice that of the direct RBF collocation method.

6.3.1 RBFs and the Particular Solutions

In this work, the types of radial basis functions can be chosen as needed, but the corresponding differentiations and integrations are required for the closed form particular solutions of

RBFs in both global and local cases of Kansa method and MAPS. In this paper, we use the normalized multiquadric (NMQ) RBF

$$\psi(r) = \sqrt{\varepsilon^2 r^2 + 1}$$

in 2D and the corresponding related functions listed below. For the Kansa method, the derivation of the particular solution for the Laplacian is given by,

$$\Delta\psi(r) = \frac{\varepsilon^2(\varepsilon^2 r^2 + 2)}{(\varepsilon^2 r^2 + 1)^{\frac{3}{2}}}.$$

For the direct RBF collocation method, by direct differentiation we have,

$$\Delta^2\psi(r) = \frac{\varepsilon^4(\varepsilon^4 r^4 + 8\varepsilon^2 r^2 - 8)}{(\varepsilon^2 r^2 + 1)^{\frac{7}{2}}}.$$

For the Neumann B.C., we have

$$\frac{1}{r}\frac{\partial\psi}{\partial r} = \frac{\varepsilon^2}{\sqrt{1 + (\varepsilon r)^2}}.$$

For the method of approximate particular solutions (MAPS), the derivation of particular solutions for the Laplacian by inverse differentiation is given by [50],

$$\phi = \frac{1}{9}r^2\sqrt{1+\varepsilon^2 r^2} + \frac{4}{9\varepsilon^2}\sqrt{1+\varepsilon^2 r^2} - \frac{1}{3\varepsilon^2}\log(\sqrt{1+\varepsilon^2 r^2}+1).$$

For the Neumann B.C., we have

$$\frac{1}{r}\frac{\partial\phi}{\partial r} = \frac{2\sqrt{1+\varepsilon^2 r^2} + \varepsilon^2 r^2(\sqrt{1+\varepsilon^2 r^2}+1) + 1}{3(\varepsilon^2 r^2 + \sqrt{1+\varepsilon^2 r^2}+1)}.$$

For the Biharmonic operator [50],

$$\begin{aligned}\phi &= \frac{4r^2}{75\varepsilon^2}\sqrt{1+\varepsilon^2 r^2} + \frac{r^2}{12\varepsilon^2} - \frac{61}{900\varepsilon^4}\sqrt{1+\varepsilon^2 r^2} \\ &\quad -\frac{r^2}{12\varepsilon^2}\log(\sqrt{1+\varepsilon^2 r^2}+1) + \frac{r^4}{225}\sqrt{1+\varepsilon^2 r^2} + \frac{\log(\sqrt{1+\varepsilon^2 r^2}+1)}{30\varepsilon^4}.\end{aligned}$$

For the Neumann B.C., we have

$$\begin{aligned}\frac{1}{r}\frac{\partial\phi}{\partial r} &= \frac{11}{90\varepsilon^2}\sqrt{1+\varepsilon^2 r^2} - \frac{2\log(\sqrt{1+\varepsilon^2 r^2}+1) - 1}{12\varepsilon^2} \\ &\quad + \frac{17r^2}{450\sqrt{1+\varepsilon^2 r^2}} + \frac{10\varepsilon^2 r^4 + \frac{15}{\varepsilon^2(\sqrt{1+\varepsilon^2 r^2}+1)} + 8r^2}{450\sqrt{1+\varepsilon^2 r^2}}.\end{aligned}$$

6.4 Numerical Results

To verify the effectiveness of the new approach for solving fourth order PDEs, two numerical examples are presented. We have compared the results in terms of accuracy implementing the Kansa method directly and with the new formulation employed in this paper both globally and locally. The multiquadric (MQ) is used as a basis function. The normalized form of MQ, which is called normalized the multiquadric (NMQ) has also been used as a basis function. We have also compared the errors of MQ and NMQ with the shape parameter ε. We use the leave-one-out cross validation (LOOCV) algorithm [56] to find a suitable shape parameter ε for MQ. Direct KANSA and New KANSA respectively represent the results obtained by using the Kansa method directly and by the new formulation employed in this paper in the global case. Direct LKANSA and New LKANSA respectively represent the corresponding results for the local case. Direct MAPS, New MAPS, Direct LMAPS, and New LMAPS are defined similarly for the method of approximate particular solutions both in global and local cases.

To validate the numerical accuracy, we calculate the following root mean square error (RMSE),

$$RMSE = \sqrt{\frac{1}{q}\sum_{j=1}^{q}(\hat{u}_j - u_j)},$$

where q is the number of testing nodes chosen randomly in the domain, u_j and $\hat{u}_j$ denote the exact solution and approximate solution at the j^{th} node, respectively. In the numerical results, n_i and n_b respectively represent the number of interior and boundary points.

6.4.1 Example 1

We consider the following partial differential equation with mixed boundary conditions:

$$\begin{aligned} Lu(x,y) &= f(x,y), \ \ (x,y) \in \Omega, \\ u(x,y) &= \sin(\pi x)\cosh(y) - \cos(\pi x)\sinh(y), \ \ (x,y) \in \partial\Omega, \\ \frac{\partial u(x,y)}{\partial \mathbf{n}} &= g(x,y)\dot{\boldsymbol{n}}, \ \ (x,y) \in \partial\Omega, \end{aligned} \tag{6.12}$$

where

$$L = \Delta^2 + x^2y^3 + y\cos(y)\frac{\partial}{\partial x} + \sinh(x)\frac{\partial}{\partial y},$$

and $\dot{\boldsymbol{n}}$ is the unit normal vector. $f(x,y)$ and $g(x,y)$ are generated from the analytical solution:

$$u(x,y) = \sin(\pi x)\cosh(y) - \cos(\pi x)\sinh(y).$$

The computational domain Ω as shown in Figure 6.1 is bounded by the curve defined by the parametric equation:

$$\partial\Omega = \{(x,y)|x = \rho\cos\theta, y = \rho\sin\theta,\ 0 \leq \theta \leq 2\pi\},$$

where

$$\rho = e^{\sin\theta}\sin^2(2\theta) + e^{\cos\theta}cos^2(2\theta).$$

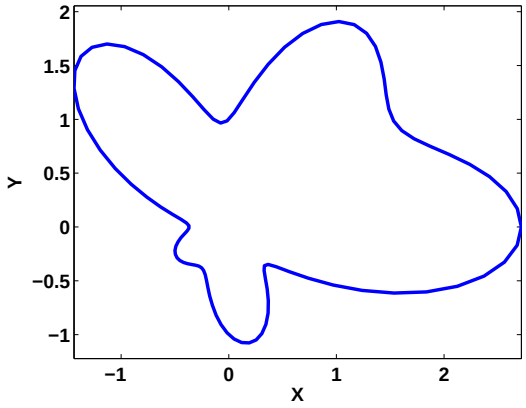

Figure 6.1: Amoeba-shaped Domain.

Table 6.1: RMSE for New LMAPS and Direct LMAPS.

	New LMAPS			Direct LMAPS		
(ni,nb)	RMSE	CPU Time	ε	RMSE	CPU Time	ε
(3809,500)	2.330e-03	5.95	1.52	9.030e-03	4.19	1.62
(15254,500)	2.630e-05	25.29	1.87	4.950e-03	15.40	1.65
(23850,500)	9.510e-06	40.13	2.54	2.770e-02	23.82	3.10

We list in Table 6.1 the numerical results for the LMAPS with Ω being an amoeba-shape domain. Numerical accuracy between New LMAPS and Direct LMAPS is almost the same for a small number of interior nodes. However, as the number of interior nodes increases, the New LMAPS is far superior than the direct one. Due to the large size of the matrix in the new formulation, the computational cost is slightly higher than the Direct LMAPS, which seems reasonable. The number of interior points is taken up to $23,850$ with 500 boundary points with an accuracy of 9.510×10^{-6} which is promising. We chose 21 nodes in the local domain. The stability of the normalized MQ as depicted in Figure 6.2 enables us to find the stable solution in the New LMAPS by LOOCV. We observe the same kind of stability behavior in the Direct LMAPS as shown in Figure 6.3.

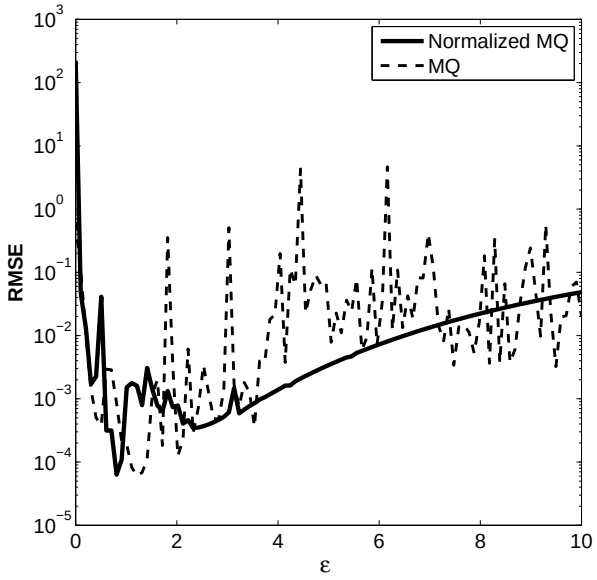

Figure 6.2: MQ versus NMQ in New LMAPS.

Table 6.2: RMSE for New LKANSA and Direct LKANSA using NMQ.

	New LKANSA		Direct LKANSA	
(ni,nb)	RMSE	ε	RMSE	ε
(3809,500)	3.673e-01	3.72	4.269e-02	2.36
(15254,500)	4.451e-04	4.67	1.227e-02	2.31
(23850,500)	6.311e-04	5.74	3.438e-02	3.11

We compare the numerical accuracy of the new local Kansa method and direct local Kansa method in Table 6.2 with the same number of computational nodes as in Table 6.1. From the numerical results, we can easily observe that the new approach performed better than the direct one. Moreover, in this paper we wanted to compare the performance of NMQ over MQ. From Figures 6.2 and 6.3, we can easily observe that NMQ seems to have more stable results as compared to the results obtained from MQ.

Table 6.3: RMSE for New MAPS and Direct MAPS using NMQ.

	New MAPS		Direct MAPS	
(ni,nb)	ε	RMSE	ε	RMSE
(60,30)	0.40	4.277e-04	0.35	1.361e-03
(126,60)	0.61	1.089e-04	0.71	5.600e-04
(208,90)	0.91	3.696e-05	1.41	1.665e-04
(507,180)	1.72	4.204e-05	2.47	1.056e-04

Tables 6.3 and 6.4 show the numerical results for the global RBF collocation methods such as Kansa method and MAPS. We compared the numerical accuracy between the new formulation and direct ones. We tested $60, 126, 208$, and 507 different interior points for the amoeba-shape domain. When we increased the number of computational nodes, the new formulation performed better than the direct ones in both cases. In this case, we used 507 interior points, 180 boundary points, and 300 test points. The new MAPS has accuracy of 4.204×10^{-5} at shape parameter 1.72 and the new Kansa method has accuracy of 4.050×10^{-5} at shape parameter 1.32 which is at least one order of accuracy better than the corresponding direct ones for 507 interior nodes and 180 boundary nodes. From this observation, we can easily say that this new approach is equally suitable for global collocation methods also.

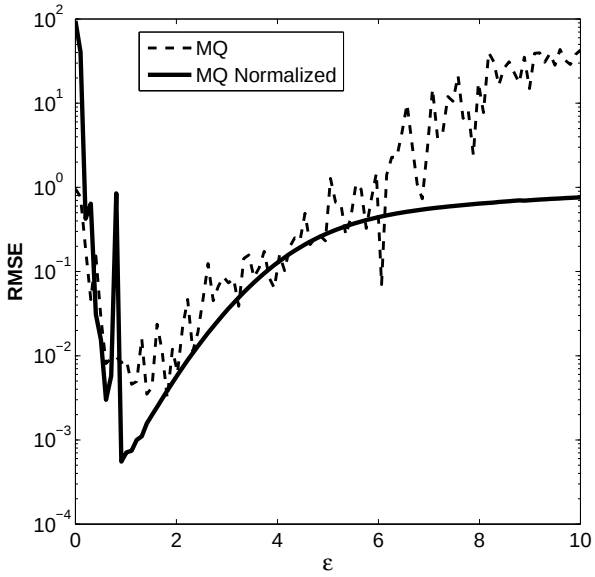

Figure 6.3: MQ versus NMQ in Direct LMAPS.

Table 6.4: RMSE for New KANSA and Direct KANSA using NMQ.

	New KANSA		Direct KANSA	
(ni,nb)	ε	RMSE	ε	RMSE
(60,30)	0.30	1.666e-04	0.71	2.304e-02
(126,60)	0.56	1.752e-04	0.91	1.583e-03
(208,90)	0.81	9.363e-05	1.01	2.411e-04
(507,180)	1.36	4.050e-05	1.01	1.474e-04

6.4.2 Example 2

We consider the following convection-diffusion equation:

$$\begin{aligned} Lu(x,y) &= f(x,y), \ (x,y) \in \Omega, \\ u(x,y) &= y\sin(x) + x\cos(y), \ (x,y) \in \partial\Omega, \\ \Delta u(x,y) &= g(x,y), \ (x,y) \in \partial\Omega, \end{aligned} \tag{6.13}$$

where

$$L = \Delta^2 + xy + 2y\sin(x)\frac{\partial}{\partial x} - y\cos(x)\frac{\partial}{\partial y},$$

$f(x,y)$ and $g(x,y)$ are generated from the analytical solution:

$$u(x,y) = y\sin(x) + x\cos(y).$$

The computational domain is bounded by the following peanut-shaped parametric curve as shown in Figure 6.4 :

$$\partial\Omega = \{(x,y) | x = \rho\cos\theta, y = \rho\sin\theta, \ 0 \le \theta \le 2\pi\},$$

where

$$\rho = \left(\cos(2\theta) + \sqrt{(1.1 - \sin^2(2\theta))}\right).$$

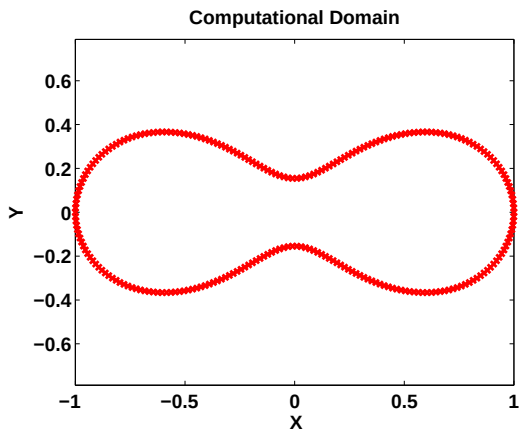

Figure 6.4: Peanut-shaped Domain.

In Tables 6.5 and 6.6, we compared the numerical results of global RBF collocation methods. In this example, we tested fewer computational nodes as compared to the previous example. For the Kansa method, just by using 293 interior points and 120 boundary points, the accuracy for the new Kansa method is 3.059×10^{-7}. Similar accuracy is obtained

for the new MAPS with the same number of computational nodes. Due to the smooth boundary of the peanut-shape domain, the accuracy shows an improvement compared to the amoeba-shape domain which we can observe from the numerical results. In this example also, we observed that the new method performed at least one order of accuracy better than the direct ones. Moreover, from the result, we see that the accuracy is improving quickly as the number of interior and boundary nodes increases.

Table 6.5: RMSE for New KANSA and Direct KANSA using NMQ.

	New KANSA		Direct KANSA	
(ni,nb)	ε	RMSE	ε	RMSE
(25,20)	0.20	2.204e-06	0.22	4.656e-04
(145,60)	0.07	2.552e-07	0.36	8.398e-06
(293,120)	0.12	3.059e-07	0.37	8.111e-06

Table 6.6: RMSE for New MAPS and Direct MAPS using NMQ.

	New MAPS		Direct MAPS	
(ni,nb)	ε	RMSE	ε	RMSE
(25,20)	0.25	3.394e-06	0.20	5.315e-05
(145,60)	1.01	2.541e-07	0.43	7.622e-06
(293,120)	1.62	2.047e-07	0.86	6.248e-06

The numerical results of the fourth-order convection-diffusion equation for local Kansa method and local MAPS are listed in Tables 6.7 and 6.8, respectively. In this example, we used 15 points in the local subdomain. To solve this Dirichlet problem, we used different numbers of interior and boundary nodes using the normalized MQ. Here we can observe that for only 1602 interior points and 80 boundary points, the accuracy for the new local Kansa method and direct local Kansa method are 1.761×10^{-6} and 4.584×10^{-4}, respectively, which are considerably good. As we increase the interior and boundary nodes the accuracy reaches 2.144×10^{-7} for the new local Kansa method, which is even better than the new LMAPS. From this numerical result we can assert that the new approach is equally applicable for the convection-diffusion equation.

6.5 Conclusions

Solving fourth-order PDEs with high accuracy and efficiency is not an easy task. By using an intermediate step to reduce fourth-order PDEs to second-order PDEs, we successfully implemented the new approach to solve various PDEs including convection-diffusion equations.

Table 6.7: RMSE for New LKANSA and Direct LKANSA using NMQ.

	New LKANSA		Direct LKANSA	
(ni,nb)	ε	RMSE	ε	RMSE
(1602,80)	1.11	1.761e-06	0.51	4.584e-04
(2024,120)	0.91	1.010e-06	0.40	1.841e-04
(2508,180)	1.01	2.144e-07	0.35	1.039e-04

Table 6.8: RMSE for New LMAPS and Direct LMAPS using NMQ.

	New LMAPS		Direct LMAPS	
(ni,nb)	ε	RMSE	ε	RMSE
(1602,80)	1.31	1.896e-06	0.66	1.088e-04
(2024,120)	1.62	1.059e-06	0.71	4.083e-05
(2508,180)	1.62	8.752e-07	0.10	5.458e-05

Numerical results show that the new formulation of RBF collocation methods outperformed the direct RBF collocation methods both in global and local cases. Here, we would like to emphasis the fact that the matrix size in the new formulation is twice that of the direct formulation, however, it is still efficient and accurate. From the numerical results, we observe that the new formulation has at least one order of accuracy better than the direct ones. Moreover, the use of the normalized MQ seems to have very stable results compared to the results obtained by MQ. LOOCV is able to catch the optimal shape parameter due to the stability of the normalized MQ even in the local case.

Chapter 7

CONCLUSIONS AND FUTURE WORKS

7.1 Conclusions

It is well-known that Chebyshev polynomials are valuable tools in the numerical analysis and approximation theory. In particular, they are widely used in the numerical solution of boundary value problems for partial differential equations with spectral methods. In this dissertation, hybrid Chebyshev polynomial scheme (HCPS) is proposed which is applied in one-step approach and two-step approach to solve various types of partial differential equations.

In two-step HCPS approach, first, Chebyshev polynomials are used to approximate a particular solution of a PDE. Then, the resulting homogeneous equations are solved by boundary type methods including the method of fundamental solution (MFS) and the collocation Trefftz method (CTM). Although radial basis functions (RBF) such as multiquadrics (MQ), inverse multiquadrics (IMQ), Gaussian have been used as candidates for approximating particular solutions in meshless methods, they often suffer from the ill-conditioned problem. In general, the matrix we obtain while using the CTM is ill-conditioned. So, proper care should be given while solving the system. Equilibrated collocation Trefftz method is employed in this dissertation to address the ill-conditioning of the CTM. Due to the nature of the Chebyshev polynomials, this numerical scheme can be easily extended to problems in high-dimensional spaces. This method was successfully tested on second and fourth order elliptic PDEs with constant coefficients in various irregular domains.

On the other hand, one-step hybrid Chebyshev polynomial scheme can be applied to solve even more larger class of PDEs. In this method, two matrix systems in the two-step HCPS is combined into a one-step only. The solution is approximated by the sum of the particular solution and homogeneous solution. Chebyshev polynomials are used to approximate a particular solution of a PDE. Various elliptic PDEs with variable coefficients were successfully solved by this method. Numerical results show that both approaches are highly accurate, stable, and efficient.

In spite of the simplicity and accuracy of the both proposed methods, they have their own limitations like many other numerical techniques. To apply this method, it is assumed that the forcing term $f(x,y)$ can be smoothly extended to a rectangular domain which contains

the given domain. Otherwise, the basis functions that work for scattered data is more appropriate for finding particular solutions.

It is highly challenging task to develop a numerical method which is highly accurate, stable, and efficient. The performance of this proposed method is far better than the similar methods in the meshless literature such as two-stage MFS-MPS, one-stage MFS-MPS and the Kansa method. We compared the numerical accuracy of the radial basis function collocation methods and the Chebyshev collocation method in this dissertation. The ill-conditioning of the matrix if it occurs is due to the MFS and the CTM. However, proper care was given in this dissertation to alleviate that problem. There is no problem of ill-conditioning while using Chebyshev polynomials.

The MFS and the CTM are highly accurate boundary alone meshless methods. In this dissertation, the performance of the MFS and the CTM is compared in various elliptic PDEs. Numerical examples showed that the performance of the CTM is slightly better than the MFS. It is always a challenging task to implement a numerical scheme in higher dimensions. Hybrid Chebyshev polynomial scheme is successfully employed in three dimensional domains such as Stanford Bunny, unit sphere, double-sphere, and bumpy-sphere. Our numerical scheme is also implemented to solve Cauchy-Navier equations of elasticity in the unit square. The merits of using hybrid Chebyshev polynomial scheme in this dissertation are summarized as follows:

- the convergence rate of MFS-MPS method is highly improved due to the use of Chebyshev polynomials.
- the use of Chebyshev polynomials addressed the problem of ill-conditioning which often occurs when RBFs are used.
- the numerical accuracy by this method is much higher than that by any other RBF techniques.
- the proposed scheme can even handle a matrix size upto 27000×27000, with a good accuracy which indeed is a big achievement.

7.2 Future Works

Hybrid Chebyshev polynomial scheme (HCPS), introduced in this dissertation can be used for solving large class of problems in science and engineering. To verify the accuracy of the proposed numerical method, various numerical examples were performed and compared with the similar RBF methods in the literature. Standing on the sound theoretical background of the Chebyshev polynomials, the following topics are of particular interest:

- Time dependent partial differential equations (PDEs) are another large class of problems in science and engineering. One-stage MFS-MPS has already been applied to solve various time dependent problems. So, two-step and one-step hybrid Chebyshev polynomial scheme (HCPS) can also be extended to solve various time dependent problems.

- Most recently, Nath *et al.* [53] used one-stage MFS-MPS for the steady Navier-Stokes equations in a lid-driven cavity. We expect to implement our numerical scheme to solve similar problems in fluid dynamics and other related fields.

- Many fluid dynamic problems and other real world physical phenomena are mostly modeled by nonlinear PDEs. The collocation techniques employed in this proposed method suggests that this method can be available for the solution of many nonlinear PDEs, if the currently documented efficiency can be maintained.

- Many numerical schemes are developed to solve axisymmetric problems. Standing on the well documented theory and spectral convergence of the Chebyshev polynomials, we are very optimistic to implement our numerical scheme to solve axisymmetric problems.

- In this dissertation, we successfully used Chebyshev polynomials as a basis function to approximate the particular solution of a PDE. There are other othogonal polynomials such as Jacobi polynomials, Laguerre polynomials, Hermite polynomials, and Legendre polynomials which have been widely used in Mathematics for years. So, the viability of using these orthogonal polynomials in this numerical work is our future project.

- Finally, issues of convergence, efficiency, consistency, and stability remain to be analyzed. However, HCPS is proven to be a highly accurate, stable, and very efficient global method to solve various elliptic PDEs. So, to handle a large number of data sets and a wide variety of PDEs, devising localized methods of our numerical scheme is our future goal.

BIBLIOGRAPHY

[1] http://graphics.stanford.edu/data/3dscanrep/.

[2] K.E. Atkinson. The numerical evaluation of particular solutions for Poisson's equation. 5:319–338, 1985.

[3] J.P. Boyd. *Chebyshev and Fourier Spectral Methods*. Dover, New York, 2000.

[4] M.D. Buhmann. *Radial Basis Functions, Theory and Implementations*. Cambridge University Press, 2003.

[5] C. Canuto, M.Y. Hussaini, A. Quarteroni, and A. H-D. Cheng. *Spectral Methods in Fluid Dynamics*. Springer-Verlag, Berlin, 1988.

[6] C.S. Chen, C.M. Fan, and P.H. Wen. The method of particular solutions for solving elliptic problems with variable coefficients. *The International Journal for Numerical Methods in Biomedical Engineering*, 8:545–559, 2011.

[7] C.S. Chen, C.M. Fan, and P.H. Wen. The method of particular solutions for solving certain partial differential equations. *Numerical Methods for Partial Differential Equations*, 28:506–522, 2012. doi: 10.1002/num.20631.

[8] C.S. Chen, M.A. Golberg, M. Ganesh, and A.H.-D. Cheng. Multilevel compact radial functions based computational schemes for some elliptic problems. *Computers and Mathematics with Application*, 43:359–378, 2002.

[9] C.S. Chen, A. Karageorghis, and Y. Li. On choosing the location of the sources in mfs. *Numer. Algorithms*, Vol 72, 1, PP 107-130, 2016.

[10] C.S. Chen, S.W. Lee, and C.-S. Huang. Derivation of particular solution using chebyshev polynomial based functions. *International Journal of Computational Methods*, 4(1):15–32, 2007.

[11] C.S. Chen, A.S. Muleshkov, and M.A. Golberg. The numerical evaluation of particular solution for Poisson's equation - a revisit. In C.A. Brebbia and H. Power, editors, *Boundary Elements XXI*, pages 313–322. WIT Press, 1999.

[12] W. Chen, Z. Fu, and C.S. Chen. *Recent advances in Radial basis Function Collocation Methods*. Springer, 2013.

[13] W. Chen and M. Tanaka. New insights into boundary-only and domain-type RBF methods. *Int. J. Nonlinear Sci. & Numer. Simulation*, 1:145–151, 2000.

[14] W. Chen and M. Tanaka. A meshless, integration-free, and boundary-only rbf technique. *Comput. Math. Appl.,43(3-5):379-91*, 2002.

[15] W. Chen and F.Z. Wang. A method of fundamental solutions without fictitious boundary. *Eng. Anal. Boundary Elements,34(5):530-2*, 2010.

[16] A.H.-D. Cheng. Particular solutions of laplacian, helmholtz-type, and polyharmonic operators involving higher order radial basis functions. *Eng. Analy. Boundary Elements*, 24:531–538, 2000.

[17] J. Ding, H. Tian, and C.S. Chen. The derivation of particular solutions using chebyshev polynomials. *Eng. Anal. Boundary Elements*, 2007.

[18] G. Fairweather and A. Karageorghis. The method of fundamental solution for elliptic boundary value problems. *Advances in Computatonal Mathematics*, 9:69–95, 1998.

[19] G. Fasshauer. Solving partial differential equations by collocation with radial basis functions. *Proceedings of Chamonix pp 1-6*, 1996.

[20] G. Fasshauer. *Meshfree Application Method with Matlab*. Interdisciplinary Mathematical Sciences, 2007.

[21] G. Fasshauer and G. Liu. *Meshfree methods: moving beyond the finite element method.* CR Press: Boca Raton,, 2007.

[22] B. Fornberg and G. Wright. Stable computation of multiquadric interpolants for all values of the shape parameter. *Comput. Math. Appl., 853-867*, 2004.

[23] L. Fox and I. B. Parker. *Chebyshev Polynomias in Numerical Analysis*. Oxford University Press, London, 1968.

[24] L. Fox, I.B. Parker, and C.B. Moler. Approximations and bounds for eigenvalues of elliptic operators. *sIAM J. Numer. Anal. 4:89-102*, 1967.

[25] R. Franke. Scattered data interpolation: tests of some methods. *Mathematics of Computation*, 48:181–200, 1982.

[26] Z-J. Fu, W. Chen, and L. Ling. Method of approximate particular solutions for constant- and variable-order fractional diffusion models. *Eng. Anal. Boundary Elements, 57, 37-46*, 2015.

[27] M.A. Golberg and C.S. Chen. The method of fundamental solutions for potential, Helmholtz and diffusion problems. In M.A. Golberg, editor, *Boundary Integral Methods: Numerical and Mathematical Aspects*, pages 103–176. WIT Press, 1998.

[28] M.A Golberg, A.S. Muleshkov, C.S. Chen, and A.H.-D. Cheng. Polynomial particular solutions for certain kind of partial differential operators. *Numerical Methods for Partial Differential Equations*, 19:112–133, 2003.

[29] D. Halpern, O. E. Jensen, and J. B. Grotberg. A theoretical study of surfactant and liquid delivery into the lung. *Journal Appl. Physiology*, 19:147-161, 1990.

[30] F. Hartmann. *Elastostatics, Progress in Boundary Element Methods.* Pentech Press, London, 1981, pp. 84-167.

[31] J.D. Hoffman and S. Frankel. *Numerical Methods for engineers and Scientist*. CR Press: Boca Raton,, 2001.

[32] E.J. Kansa. Multiquadrics - a scattered data approximation scheme with applications to computational fluid dynamics - I. *Comput. Math. Applic.*, 19(8/9):127–145, 1990.

[33] E.J. Kansa. Multiquadrics - a scattered data approximation scheme with applications to computational fluid dynamics - II. *Comput. Math. Applic.*, 19(8/9):147–161, 1990.

[34] A. Karageorghis and I. Kyza. Efficient algorithms for approximating particular solutions of elliptic equations using chebyshev polynomials. *Commun. Comput. Phys. Vol 2, No.3, pp.501-521*, 2007.

[35] E. Kita and N. Kamiya. Trefftz method an overview. *Advances in Engineering software,24,3-12*, 1995.

[36] C-L Kuo, W. Yeih, C. Liu, and J-R Chang. Solving helmholtz equation with high wave number and ill-posed inverse problem using the multiplescales trefftz collocation method. *Eng. Anal. Boundary Elements*, 2015.

[37] V.D. Kupradze and M.A. Aleksidze. The method of functional equations for the approximate solution of certain boundary value problems. *U.S.S.R. Computational Mathematics and Mathematical Physics*, 4:82–126, 1964.

[38] R. Leveque. *Finite Volume Methods for Hyperbolic Problems*. Cambridge University Press, 2002.

[39] W. Li, X. Liu, and G. Yao. A local meshless collocation method for solving certain inverse problems. *Eng. Anal. Boundary Elements,57, 9-15*, 2015.

[40] X. Li and C. S. Chen. A mesh-free method using hyperinterpolation and fast fourier transform for solving differential equation. *Eng. Anal. Boundary Elements,28,1253-1260*, 2004.

[41] Z-C. Li, T-T. Lu, H-Y. Hu, and A. H-D. Cheng. *Trefftz and Collocation Methods*. WIT Press, 2008.

[42] C.S. Liu. A multiple scale trefftz method for an incomplete cauchy problem of biharmonic equation. *Eng. Anal. Boundary Elements*, 37(11) 2013: 17-42.

[43] Y. J. Liu. A new boundary meshfree method with distributed source. *Eng. Anal. Boundary Elements, 34:914-9*, 2010.

[44] M. Lysaker, A. Laudervold, and X.C. Tai. Noise removal using fourth-order pde with applications to medical magnetic resonance images in space and time. *IEEE Transactions on Image Processing*, Vol 12, No. 12, 2003.

[45] N. Mai-Duy and T. Tran-Cong. Mesh-free radial basis function network methods with domain decomposition for approximation of functions and numerical solution of poisson's equation. *Eng. Anal. Boundary Elements*, 2002, 26:133-156.

[46] J. C. Mason and D.C. Handscomb. *Chebyshev Polynomials*. Chapman & Hall/CRC, Boca Raton, FL, 2003.

[47] R. Mathon and R.L. Johnston. The approximate solution of elliptic boundary-value problems by fundamental solutions. 14:638–650, 1977.

[48] T. May. *Boundary Conditions in the Numerical Integration of Hyperbolic Equations*. PhD thesis, University of Reading, Reading, May 1978.

[49] I. McCausland. *Introduction to Optimal Control*. John Wiley & Sons, 1969.

[50] J. Monroe. *Hybrid Meshless Method for Solving Partial Differential Equations*. PhD thesis, University of Southern Mississippi, 2014.

[51] K. W. Morton and D. F. Mayers. *Numerical Solution of PDEs, an Introduction*. Cambridge University Press, 2005.

[52] T. G. Myers, J. P. F. Charmin, and S. J. Chapman. A mathematical model for atmospheric ice accretion and water flow on a cold surface. *Int. J. Heat Mass Tran*, 2004.

[53] D. Nath, M.S. Kalra, and P. Munshi. One-stage method of fundamental and particular solutions (mfs-mps) for the steady navier-stokeequations in a lid-driven cavity. *Eng. Anal. Boundary Elements,58:39-47*, 2015.

[54] R. Peyret. *Spectral Methods for Incompressible Viscous Flow*. Springer-Verlag, New York, 2002.

[55] J. N. Reddy. *An Introduction to the Finite Element Method*. McGraw-Hill, Inc., 2006.

[56] S. Rippa. An algorithm for selecting a good value for the parameter c in radial basis function interpolation. *Advances in Computational Mathematics*, 11:193–210, 1999.

[57] B. Sarler. Solution of potential flow problems by modified method of fundamental solutions: formulations with the single-layer and the double-layer fundamental solution. *Eng. Anal. Boundary Elements, 33:1374-82*, 2009.

[58] B. Sarler and R. Vertnik. Meshfree explicit local radial basis function collocation method for diffusion problems. *Computers and Mathematics with Applications*, 21:1269–1282, 2006.

[59] G.D. Smith. *Numerical Solution of partial differential equations, Finite Difference Methods*. Oxford University Preox (3rd ed.), 1985.

[60] P. Solin, K. Segeth, and I. Dolozel. *Higher Order Finite Element Methods*. Chapman & Hall/CRC Press, 2003.

[61] G. Strang. *An Analysis of Finite Element Method*. Prentice Hall, 1973.

[62] A. Suli and F. D. Mayers. *An Introduction to Numerical Analysis*. Cambridge University Press, 2003.

[63] E. Trefftz. Ein gegenstück zum ritzschen verfahren. In *2. Int. Kongr. f. Techn. Mechanik, Zürich*, pages 131–137, 1926.

[64] H. Wendland. Piecewise polynomial, positive definite and compactly supported radial functions of minimal degree. 4:389–396, 1995.

[65] J. Yang, X. Liu, and P.H. Wen. The local kansa's method for solving berger equation. *EngEng. Anal. Boundary Elements,16-22*, 2015.

[66] G. Yao, J. Kolibal, and C. S. Chen. A localized approach for the method of approximate particular solutions. *Comput. Math. Appl.*, 61(9):2376–2387, May 2011.

[67] G. Yao, C. Tsai, and W. Chen. The comparison of three meshless methods using radial basis functions for solving fourth-order partial differential equations. *Eng. Anal. Boundary Elements*, 35:600-609, 2011.

[68] D.L. Young, K.H. Chen, and C.W. Lee. Novel meshless method for solving the potential problems with arbitrary domain. *Journal of Computational Physics*, 209(1):290–321, 2005.

INDEX